

# Orchestrated Excitatory and Inhibitory Learning Rules Lead to the Unsupervised Emergence of Self-sustained and Inhibition-stabilized Dynamics

## AUTHORS:

Saray Soldado-Magraner<sup>1</sup>, Rodrigo Laje<sup>2,\*</sup>, Dean V. Buonomano<sup>1,3,\*</sup>

## AFFILIATIONS:

<sup>1</sup>Department of Neurobiology, University of California, Los Angeles, CA, USA.

<sup>2</sup>Present addresses: Departamento de Ciencia y Tecnología, Universidad Nacional de Quilmes, Bernal, Argentina, and Consejo Nacional de Investigaciones Científicas y Técnicas (CONICET), Buenos Aires, Argentina.

<sup>3</sup>Department of Psychology University of California, Los Angeles, CA, USA.

\*RL and DVB are Joint Senior Authors on this work.

## **ACKNOWLEDGEMENTS**

We thank Juan Romero-Sosa and Helen Motanis for the sample traces shown in Figure 1. We thank Ben Liu, Shanglin Zhou, and Helen Motanis, for technical assistance and helpful discussions. We thank Joana Soldado-Magraner and Mike Seay for comments on the manuscript. This research was supported by NIH grant NS116589, and SSM was supported by the Swiss National Science Foundation (P2ZHP3-187943).

## ABSTRACT

Self-sustaining neural activity maintained through local recurrent connections is of fundamental importance to cortical function. We show that Up-states—an example of self-sustained, inhibition-stabilized network dynamics—emerge in cortical circuits across three weeks of *ex vivo* development, establishing the presence of unsupervised learning rules capable of generating self-sustained dynamics. Previous computational models have established that four sets of weights ( $W_{E \leftarrow E}$ ,  $W_{E \leftarrow I}$ ,  $W_{I \leftarrow E}$ ,  $W_{I \leftarrow I}$ ) must interact in an orchestrated manner to produce Up-states, but have not addressed how a family of learning rules can operate in parallel at all four weight classes to generate self-sustained inhibition-stabilized dynamics. Using numerical and analytical methods we show that, in part due to the paradoxical effect, standard homeostatic rules are only stable in a narrow parameter regime. In contrast, we show that a family of biologically plausible learning rules based on “cross-homeostatic” plasticity robustly lead to the emergence of self-sustained, inhibition-stabilized dynamics.

## 1 INTRODUCTION

2  
3 Self-sustained patterns of neural activity maintained by local recurrent excitation underlie  
4 many cortical computations and dynamic regimes, including the persistent activity  
5 associated with working memory (Fuster and Jervey, 1981; Goldman-Rakic, 1995; Wang,  
6 2001), asynchronous states (van Vreeswijk and Sompolinsky, 1998; Renart et al., 2010),  
7 and Up-states (Steriade et al., 1993; Timofeev et al., 2000). Recurrent excitation,  
8 however, also has the potential to drive pathological and epileptiform regimes  
9 (McCormick, 1989; Douglas et al., 1995; Steriade and Contreras, 1998). Converging  
10 theoretical and experimental evidence indicate that cortical circuits that generate self-  
11 sustained dynamics operate in an inhibition-stabilized regime, in which positive feedback  
12 is held in check by recurrent inhibition (Tsodyks et al., 1997; Brunel, 2000; Ozeki et al.,  
13 2009; Rubin et al., 2015; Rutishauser et al., 2015; Jercog et al., 2017; Sanzeni et al.,  
14 2020).

15  
16 At the computational level self-sustained activity and inhibition-stabilized networks are  
17 often modeled as a simplified circuit composed of excitatory ( $E$ ) and inhibitory ( $I$ )  
18 subpopulations of neurons with four classes of synaptic weights:  $W_{E \leftarrow E}$ ,  $W_{E \leftarrow I}$ ,  $W_{I \leftarrow E}$ ,  $W_{I \leftarrow I}$ .  
19 Analytical and numerical analyses have shown that these weights must obey certain  
20 theoretically well-defined relationships in order to generate self-sustained, inhibition-  
21 stabilized dynamics (Tsodyks et al., 1997; Brunel, 2000; Ozeki et al., 2009; Rubin et al.,  
22 2015; Jercog et al., 2017). Yet, it is not known how the appropriate relationships between  
23 these four classes of weights could emerge in a self-organizing manner (Sadeh and  
24 Clopath, 2021). One possibility is that standard homeostatic forms of plasticity underlie  
25 the emergence of inhibition-stabilized networks. Homeostatic learning rules generally  
26 assume that excitatory weights are regulated in a manner proportional to the difference  
27 between some ontogenetically determined set-point and average neural activity (for both  
28 excitatory and inhibitory neurons)—and conversely that inhibitory weights onto excitatory  
29 neurons are regulated in the opposite direction (Turrigiano et al., 1998; van Rossum et  
30 al., 2000; Kilman et al., 2002; Turrigiano and Nelson, 2004; Peng et al., 2010). However,  
31 it remains an open question whether homeostatic rules can lead to the self-organized  
32 emergence of self-sustained, inhibition-stabilized networks.

33  
34 At both the experimental and computational level one of the simplest and best-studied  
35 examples of self-sustained activity are Up-states (Steriade et al., 1993; Timofeev et al.,  
36 2000). Up-states are characterized by network-wide regimes in which excitatory and  
37 inhibitory neurons transiently shift from a quiescent Down-state to a depolarized state  
38 with low to moderate firing rates (Sanchez-Vives and McCormick, 2000; Neske et al.,  
39 2015; Bartram et al., 2017). Up-states occur spontaneously *in vivo* during anesthesia,  
40 slow-wave sleep, and quiet wakefulness (Steriade et al., 1993; Timofeev et al., 2000;  
41 Beltramo et al., 2013; Hromádka et al., 2013), in acute slices (Sanchez-Vives and  
42 McCormick, 2000; Shu et al., 2003; Fanselow and Connors, 2010; Sippy and Yuste, 2013;  
43 Xu et al., 2013; Sadvovsky and MacLean, 2014; Neske et al., 2015; Bartram et al., 2017),  
44 and in organotypic cultures over the course of *ex vivo* development (Plenz and Kitai, 1998;  
45 Seamans et al., 2003; Johnson and Buonomano, 2007; Kroener et al., 2009; Motanis and  
46 Buonomano, 2015; Motanis and Buonomano, 2020). Furthermore, Up-state frequency

47 appears to be homeostatically regulated—e.g., optogenetically stimulating cortical circuits  
48 over the course of days decreases Up-state frequency (Motanis and Buonomano, 2015;  
49 Motanis and Buonomano, 2020).

50  
51 Consistent with previous results we first demonstrate that Up-states emerge in both  
52 excitatory and inhibitory neurons over the course of the first few weeks of *ex vivo*  
53 development, suggesting that local cortical circuits are programmed to homeostatically  
54 generate Up-states. We next used computational models and analytical methods to  
55 explore families of homeostatic learning rules that operate in parallel at all four synapse  
56 classes and lead to self-sustained, inhibition-stabilized dynamics. We show that when  
57 driving the network towards a self-sustained, inhibition-stabilized regime, standard forms  
58 of homeostatic plasticity are only stable in a narrow region of parameter space. This is in  
59 part a consequence of the paradoxical effect—in which an *increase* in excitatory drive to  
60 inhibitory neurons produces a net *decrease* in the firing rate of those same inhibitory  
61 neurons (Tsodyks et al., 1997; Ozeki et al., 2009; Rubin et al., 2015). We next developed  
62 a family of homeostatic learning rules that include “cross-homeostatic” influences, and  
63 lead to the unsupervised emergence of Up-states in the inhibition-stabilized regime in a  
64 robust manner. These rules are consistent with experimental data and generate explicit  
65 predictions regarding the effects of manipulations of excitatory and inhibitory neurons on  
66 synaptic plasticity.

67  
68

## 69 RESULTS

70

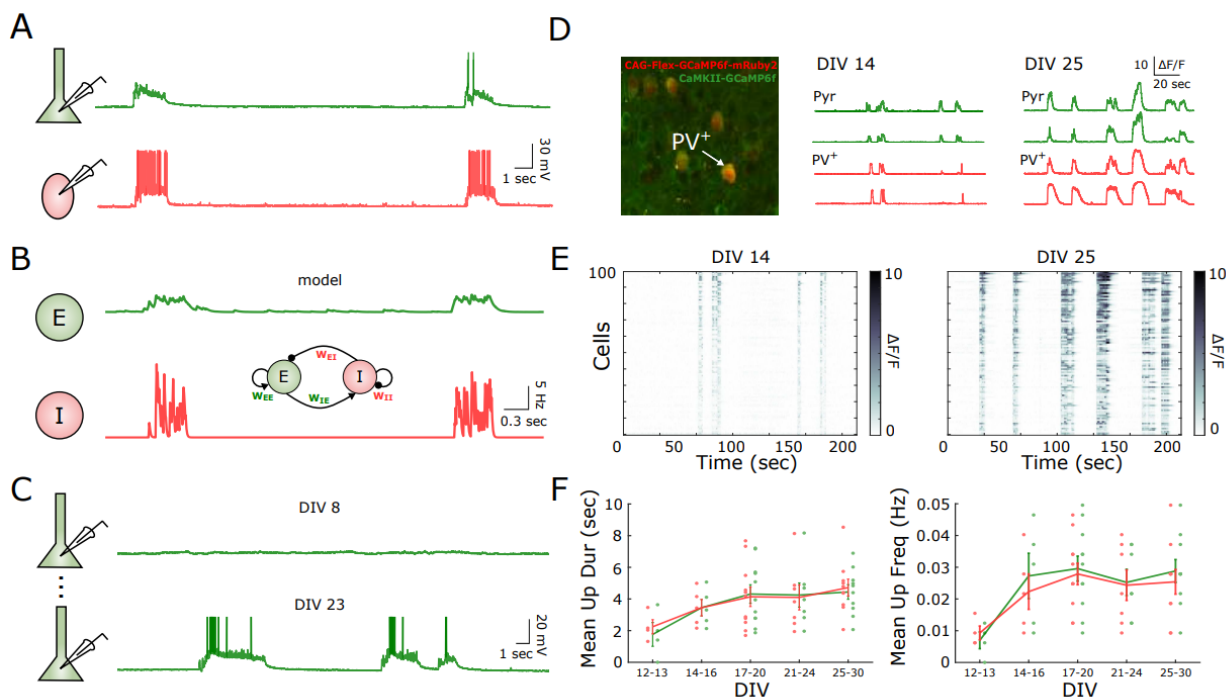
### 71 Up-states emerge autonomously during *ex vivo* development

72

73 Up-states represent a transition from a quiescent state to a self-sustained network-wide  
74 dynamic regime in which both excitatory and inhibitory neurons are active (**Fig. 1A**).  
75 During Up-states the firing rate of excitatory neurons is relatively low (1-5 Hz) indicating  
76 that recurrent excitation is held in check by appropriately tuned inhibition (Neske et al.,  
77 2015; Jercog et al., 2017; Romero-Sosa et al., 2021). Computational studies have  
78 demonstrated that Up and Down states can be simulated as a bistable dynamical system  
79 composed of interconnected populations of excitatory (*E*) and inhibitory (*I*) neurons (**Fig.**  
80 **1B**), in which Down-states represent a quiescent fixed point, and Up- or asynchronous  
81 states represent a second, non-trivial fixed-point attractor. In the Up regime recurrent  
82 excitation produces amplification, but the activity is held in check by rapid inhibition. The  
83 dynamics settles into a stable fixed-point attractor, and instantiates an example of an  
84 inhibition-stabilized network. The neural dynamics within two-population models is  
85 governed by four classes of synaptic weights  $W_{E \leftarrow E}$ ,  $W_{E \leftarrow I}$ ,  $W_{I \leftarrow E}$ ,  $W_{I \leftarrow I}$  (**Fig. 1B**, inset).  
86 Analytical and numerical studies have demonstrated that these four weights must obey  
87 certain “balanced” relationships in order to support the stable self-sustaining dynamics—  
88 e.g., if excitation is too strong, runaway (or saturated) excitation occurs, whereas if  
89 inhibition is too strong only the trivial quiescent fixed point will be stable (Tsodyks et al.,  
90 1997; van Vreeswijk and Sompolinsky, 1998; Brunel, 2000; Ozeki et al., 2009; Rubin et  
91 al., 2015; Jercog et al., 2017) (see **Section 2.2** in the Supplementary Material).

92

93 In most computational models the set of four weights is determined analytically or through  
 94 numerical searches. In contrast, recordings in cortical organotypic cultures show that Up-  
 95 states autonomously develop over the course of *ex vivo* development (Plenz and Kitai,  
 96 1998; Seamans et al., 2003; Johnson and Buonomano, 2007; Kroener et al., 2009;  
 97 Motanis and Buonomano, 2015; Motanis and Buonomano, 2020). Early in development,  
 98 at 8 days-in-vitro (DIV-8) most of the neurons are silent, while at later stages (DIV-23)  
 99 spontaneous Up-states are observed (**Fig. 1C**). Here we further characterized the  
 100 emergence of Up-states and asked whether the development of activity is in sync for both  
 101 excitatory and inhibitory neurons. Using two-photon calcium imaging, we recorded the  
 102 spontaneous activity in excitatory neurons and PV<sup>+</sup>-inhibitory neurons by expressing  
 103 GCamp6f under the CaMKII and Flex promoters in organotypic cultures of PV-Cre mice.  
 104 Calcium imaging at DIV 12-13 revealed infrequent and short bouts of synchronous  
 105 activity. By DIV 14-16 Up-states were observed, and over the entire four-weeks of *ex vivo*  
 106 development there was an increase and stabilization of Up-state frequency and duration  
 107 in both excitatory and inhibitory neurons (**Fig. 1D-F**)—suggesting the Up-states emerge  
 108 in a co-dependent manner in both populations.  
 109  
 110



111 **Figure 1. Up-states emerge autonomously over the course of *ex vivo* development.**

- 112 (A) Example of Up-states in simultaneously whole-cell recordings of a pyramidal (green) and parvalbumin (PV)  
 113 positive inhibitory neuron (red).  
 114 (B) Two-population firing rate model of Up-states. The schematic of the model is shown in the inset. The dynamics  
 115 of the excitatory (green) and inhibitory (red) populations are governed by four synaptic weights,  $W_{E-E}$ ,  $W_{E-I}$ ,  
 116  $W_{I-E}$ , and  $W_{I-I}$ . Traces correspond to the firing rate of each of the populations in the presence of external  
 117 noise.  
 118 (C) Spontaneous activity recording of a pyramidal neuron at 8 and 23 days *in vitro* development (DIV). Up-states  
 119 are present only at later developmental stages.  
 120 (D) Two-photon calcium imaging recording of excitatory and PV<sup>+</sup> neurons at different stages of development.  
 121 Organotypic slices of Cre-PV mice were transfected with pAAV-CAG-Flex-GCamp6f-mRuby2 and pAAV-  
 122 CaMKII-GCamp6f. Image shows an example slice with a PV<sup>+</sup> neuron expressing both, GCamp6f and the  
 123

124 mRuby2 red marker. Traces show the spontaneous calcium activity of 2 example PV<sup>+</sup> and excitatory cells at  
125 14 and 25 DIV. Up-states can be observed more prominently at later stages (see Methods for the definition  
126 and quantification of Up-states).  
127 (E) Spontaneous calcium activity of 100 example cells at 14 and 25 DIV. Synchronous activity events correspond  
128 to Up-states.  
129 (F) Evolution of the mean Up-state duration and frequency over the course of *ex vivo* development for excitatory  
130 (green) and PV<sup>+</sup> neurons (red). A significant increase in mean Up duration (Two-way ANOVA:  $F_{4,64} = 3.54$ ,  $p$   
131  $= 0.011$ ) and frequency (Two-way ANOVA:  $F_{4,64} = 4.75$ ,  $p = 0.002$ ) was observed over developmental time,  
132 with no statistical effect of neuron type ( $F_{4,64} = 0.13$ ,  $p = 0.97$ ) or interaction effect ( $F_{4,64} = 0.09$ ,  $p = 0.98$ ).

133  
134 The observation that Up-states emerge autonomously during *ex vivo* development  
135 indicates that synaptic learning rules are in place to orchestrate the unsupervised  
136 emergence of Up-states. Since Up-states emerge autonomously over the course of  
137 development in *ex vivo* cortical networks, and because all four weight classes have been  
138 observed to undergo synaptic plasticity in experimental studies, we next asked how the  
139 stable self-sustained dynamics characteristic of Up-states might emerge in a self-  
140 organizing manner.

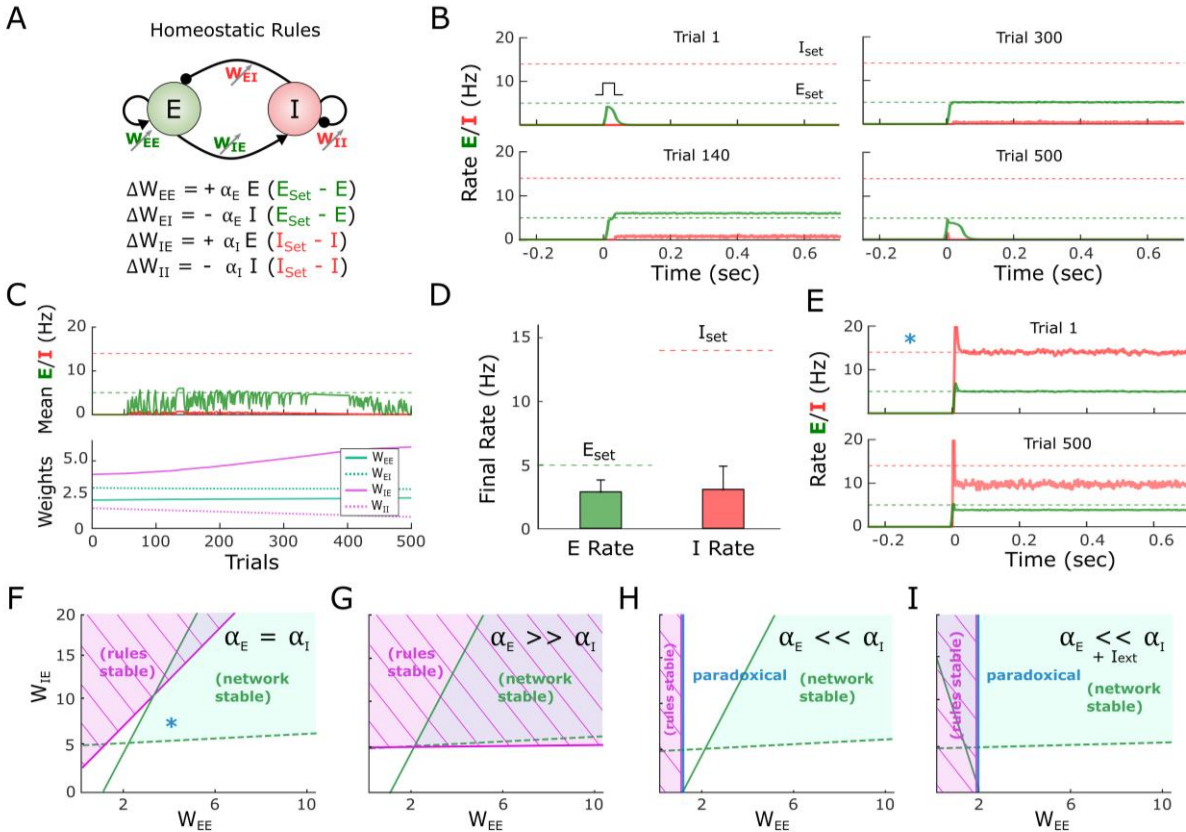
### 141 142 **Standard homeostatic learning can only account for stable self-sustained activity** 143 **in a narrow parameter regime**

144  
145 One attractive possibility is that cortical neurons are homeostatically programmed to  
146 generate Up-states. Specifically, that both excitatory and inhibitory neurons exhibit  
147 ontogenetically programmed firing rate setpoints during Up-states, and they  
148 homeostatically adjust their excitatory and inhibitory weights to reach these target  
149 setpoints. Homeostatic learning rules are traditionally defined by changes in synaptic  
150 weights that are proportional to an “error term” defined by the difference between the  
151 setpoint and the neurons average activity levels (Turrigiano et al., 1998; van Rossum et  
152 al., 2000; Kilman et al., 2002; Turrigiano and Nelson, 2004; Liu and Buonomano, 2009;  
153 Peng et al., 2010; Vogels et al., 2011), e.g.,  $\Delta W_{E \leftarrow E} \propto E_{set} - E_{avg}$  where any departure of  
154 the excitatory activity  $E_{avg}$  from the setpoint  $E_{set}$  would lead to a compensatory correction  
155 in the value of the weight  $W_{E \leftarrow E}$ .

156  
157 We first asked is stable self-sustained dynamics can emerge in a standard two-  
158 population model (Jercog et al., 2017; see Methods) through homeostatic mechanisms.  
159 We initialized the four weights ( $W_{E \leftarrow E}$ ,  $W_{E \leftarrow I}$ ,  $W_{I \leftarrow E}$ ,  $W_{I \leftarrow I}$ ) of the model at random values  
160 and applied a standard family of homeostatic learning rules to all four weights classes  
161 (**Fig. 2A**). It is well established that PV<sup>+</sup>-inhibitory neurons have higher firing rates than  
162 pyramidal neurons during Up-states (Neske et al., 2015; Romero-Sosa et al., 2021), thus  
163 based on experimental data we set the setpoints for the *E* and *I* populations during Up-  
164 states to 5 and 14 Hz, respectively (Romero-Sosa et al., 2021). We first asked whether  
165 the set of four standard homeostatic learning rules can lead to stable self-sustained  
166 dynamic regime (representing a permanent Up-state) in response to a brief external input  
167 (low levels of noise were used to avoid spontaneous Up $\leftrightarrow$ Down transitions).

168





169  
 170 **Figure 2. Standard homeostatic rules are only stable in a narrow parameter regime.**  
 171 **(A)** Schematic (top) of the population rate model in which the four weights are governed by a family of  
 172 homeostatic learning rules (bottom).  
 173 **(B)** Example simulation of the network over the course of simulated development. Each plot shows the  
 174 firing rate of the excitatory and inhibitory population over the course of a trial in response to a brief  
 175 external input.  $E_{set}=5$  and  $I_{set}=14$  represent the target homeostatic setpoints. Weights were initialized to  
 176  $W_{EE}=2.1$ ,  $W_{EI}=3$ ,  $W_{IE}=4$ , and  $W_{II}=2$ . Note that while an evoked Up-state emerges by Trial 200 the firing  
 177 rates do not converge to their setpoints, and by Trial 500 the Up-state is no longer observed.  
 178 **(C)** Average rate across trials (upper plot) for the excitatory and inhibitory populations for the data shown  
 179 in (B). Weight dynamics (bottom plot) produced by the homeostatic rules across trials for the data  
 180 shown in (B).  
 181 **(D)** Average final rate for 100 independent simulations with different weight initializations. Data represents  
 182 mean  $\pm$  SEM.  
 183 **(E)** Simulation of a network starting with weights that generate Up-states that match the  $E_{set}=5$  and  $I_{set}=14$   
 184 Hz setpoints (Trial 1, top). After 500 trials the network has diverged from its setpoints, indicating the  
 185 synaptic learning rules are unstable. Weights were initialized to  $W_{EE}=5$   $W_{EI}=1.09$   $W_{IE}=10$   $W_{II}=1.54$ .  
 186 **(F)** Analytical stability regions of the neural and learning rule subsystems as a function of the free weights  
 187  $W_{EE}$  and  $W_{IE}$ . (note that once a  $W_{EE}$  and  $W_{IE}$  are set to generate an Up-state with specific  $E_{set}$  and  $I_{set}$   
 188 values,  $W_{EI}$  and  $W_{II}$  are fully determined by  $W_{EE}$  and  $W_{IE}$ , respectively). Here the stability plot is obtained  
 189 by considering equal learning rates for all four learning rules (as used for panels B-E). Blue asterisk  
 190 corresponds to the initial conditions shown in Panel D (top).  
 191 **(G)** Similar to F but with  $\alpha_E \gg \alpha_I$ .  
 192 **(H)** Similar to F but with but with  $\alpha_E \ll \alpha_I$ . To the right of the blue line, the network is in a paradoxical regime  
 193 (defined by the condition  $W_{EE} \cdot g_E - 1 > 0$ )  
 194 **(I)** Condition of stability of the neural system and learning rule system when the learning rate on the  
 195 inhibitory neuron dominates and an external excitatory current is applied to the excitatory neuron. The



196 current produces an enlargement of the stability region of the neural subsystem. Right of blue line  
197 shows the area where the network is in a paradoxical regime.  
198

199 Although the rules are homeostatic in nature (e.g., if  $I$  is below  $I_{set}$ , an increase of  $W_{I \leftarrow E}$   
200 and a decrease in  $W_{I \leftarrow I}$  would be induced), in the example shown in **Fig. 2B-C** the  
201 network failed to converge to a stable Up-state (**Fig. 2B-C**). Initially (Trial 1) an external  
202 input to the excitatory population does not engage recurrent activity because  $W_{E \leftarrow E}$  is too  
203 weak. By Trial 200 the weights have evolved and the brief external input triggers an Up-  
204 state, but the activities  $E$  and  $I$  do not match the corresponding setpoints—the network is  
205 in a nonbiologically observed regime in which  $E > I$ —so the weights keep evolving. By  
206 Trial 600  $E = E_{set}$  but  $I < I_{set}$ , and rather than converging to  $I_{set}$ , the network returns to a  
207 regime without an Up-state by Trial 1000. At that point both setpoint error terms have  
208 increased, leading to continued weight changes (**Fig. 2C**). Results across 100 simulations  
209 with different weight initializations (see Methods) further indicate that the standard  
210 homeostatic rules are ineffective at driving  $E$  and  $I$  towards their respective setpoints and  
211 generating stable self-sustained dynamics (**Fig. 2D**).  
212

213 To gain insights into why a family of homeostatic learning rules that might intuitively  
214 converge fails to do so, we can consider the case in which a network is initialized to a set  
215 of weights that already match  $E_{set}$  and  $I_{set}$  (**Fig. 2E**). Although the neural subsystem alone  
216 is stable at this condition (Trial 1), small fluctuations in  $E$  and  $I$  cause the homeostatic  
217 rules to drive the weight values and the average activity of the network away from the  
218 setpoints (Trial 500). It is possible to understand this instability by performing an analytical  
219 stability analysis. Specifically, a two-population network in which the weights undergo  
220 plasticity can be characterized as a dynamical system composed of two subsystems: the  
221 neural subsystem composed of the two differential equations that define  $E$  and  $I$   
222 dynamics, and the synaptic learning rule subsystem defined by the four learning rules  
223 (see **Section 2.1** in the Supplementary Material). We make use of the two very different  
224 time scales of the neural (fast) and learning rule (slow) subsystems to perform a quasi-  
225 steady state approximation of the neural subsystem; then we compute the eigenvalues  
226 of the four-dimensional learning rule subsystem, and finally get an analytical expression  
227 for the stability condition of the learning rules (see **Section 2.3** in the Supplementary  
228 Material). For the entire system to be stable, both the neural and learning rules  
229 subsystems have to be stable. For the results presented in **Fig. 2B-E** we assumed the  
230 learning rates driving plasticity onto the excitatory ( $\alpha_E$ ) and inhibitory neurons ( $\alpha_I$ ) to be  
231 equal. Under these conditions, the standard homeostatic rules are mostly unstable for  
232 biologically meaningful parameter values in which the neural system is stable. An  
233 example of this result is shown in **Fig. 2F** for a particular set of parameter values.  
234 Critically, **Fig. 2F** shows that the stability region of the neural subsystem, i.e., an inhibition-  
235 stabilized network (Ozeki et al., 2009; Jercog et al., 2017), is almost entirely within the  
236 region where the homeostatic learning rule system is unstable. Only when plasticity onto  
237 the excitatory neuron is significantly faster ( $\alpha_E \gg \alpha_I$ ) is there a substantial region of overlap  
238 between the stability of the neural and learning rules subsystems (**Fig. 2G**, see  
239 Supplementary Material, **Section 1.1**).  
240

241 Because inhibitory neurons seem to undergo homeostatic plasticity as quickly or more  
242 quickly than excitatory neurons (Keck et al., 2011; Kuhlman et al., 2013; Gainey et al.,

243 2018; Ma et al., 2019) we conclude that standard homeostatic rules by themselves do not  
244 account for the emergence of stable self-sustained and inhibition-stabilized dynamics.  
245 Similarly, a combination of analytical and numerical methods also indicates that variants  
246 of these homeostatic rules, such as synaptic scaling (Turrigiano et al., 1998; van Rossum  
247 et al., 2000; Sullivan and de Sa, 2006) are also only stable in a narrow region of parameter  
248 space (see Supplementary Material, **Section 1.5**). We next show that the inherent  
249 instability of standard homeostatic learning rules is related to the paradoxical effect.

250

## 251 **The paradoxical effect hampers the ability of homeostatic rules to lead to self-** 252 **sustained activity**

253

254 The inability of the homeostatic learning rules to generate stable Up-states is in part a  
255 consequence of the paradoxical effect, a counterintuitive, yet well described, property of  
256 two-population models of Up-states and inhibition-stabilized networks (Tsodyks et al.,  
257 1997; Ozeki et al., 2009). Specifically, if during an Up-state one increases the excitatory  
258 drive to the inhibitory population, the net result is a decrease in the firing rate of the  
259 inhibitory units. This paradoxical effect can be understood in terms of the  $I \rightarrow E \rightarrow I$  loop:  
260 the increased inhibitory drive leads to a lower steady-state rate for  $E$ , but this new steady-  
261 state value requires a decrease in the  $I$  firing rate to maintain an appropriate E/I balance  
262 (in effect, the decrease in  $E$  decreases the drive to  $I$  by more than the external increase  
263 to  $I$ ). This paradoxical effect has profound consequences for learning rules that attempt  
264 to drive excitatory and inhibitory weights to their setpoints.

265

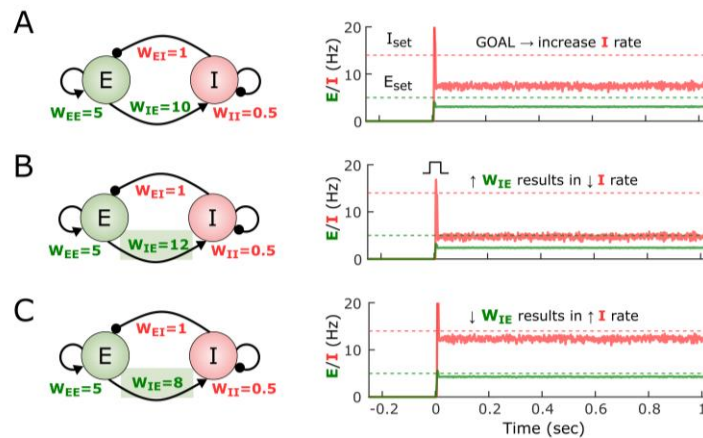
266 The relationship of the paradoxical effect and the homeostatic rules performance is  
267 presented in **Fig. 2H**. The region of stability for the homeostatic learning rules is shown  
268 in a parameter regime where inhibitory plasticity is much faster ( $\alpha_E \ll \alpha_I$ ). Contrary to  
269 when excitatory plasticity dominates, the region of stability is small, and there is no  
270 overlap with the region of stability of the neural subsystem. Crucially, the boundary of the  
271 stability region of the learning rule coincides with the condition for the paradoxical effect  
272 to be present (right of the blue line in **Fig. 2H**, see Supplementary Material, **Sections 2.2**  
273 **and 2.3**). Under these conditions, the rules can only be stable when the network is not in  
274 an inhibition-stabilized regime. If a network regime with non-zero  $E$  would be forced to  
275 exist in that region (for example, via tonic external current, **Fig. 2I**), it would only be stable  
276 in the non-paradoxical region with the learning rules in place (see **Section 2.5** in the  
277 Supplementary Material).

278

279 To understand the impact of the paradoxical effect on homeostatic learning rules  
280 consider a network state in which the  $I$  rate falls significantly below its setpoint, and the  $E$   
281 rate is close to its setpoint (**Fig. 3A**). In order to reach the  $I$  setpoint, homeostatic plasticity  
282 in the inhibitory neuron would intuitively result in an increase of  $W_{I \leftarrow E}$ . However, because  
283 of the paradoxical effect an increase in  $W_{I \leftarrow E}$  actually makes  $I$  decrease (**Fig. 3B**)—thus  
284 increasing the error term  $I_{set} - I$ . To increase the steady-state inhibitory rate we can “anti-  
285 homeostatically” decrease the excitatory weight onto the inhibitory neurons (**Fig. 3C**).  
286 This simple example shows the complexity of designing a coherent set of rules in such a  
287 coupled system (see an analysis of the paradoxical effect in **Section 2.2** of the  
288 Supplementary Material). This analysis also explains why homeostatic learning rules can

289 lead to self-sustained activity at the appropriated setpoints when  $\alpha_E \gg \alpha_I$ . Essentially by  
 290 allowing plasticity onto the  $E$  population to be faster one overcomes the counterproductive  
 291 homeostatic plasticity associated with the paradoxical effect.  
 292

293 The interaction between the paradoxical effect and homeostatic plasticity in inhibitory  
 294 neurons leads to the question of whether anti-homeostatic plasticity rules may be more  
 295 effective that standard homeostatic rules—e.g.,  $\Delta W_{I \leftarrow E} \propto -(I_{set} - I_{avg})$ . Thus, we also  
 296 examined a number of hybrid families of learning rules with different combinations of  
 297 homeostatic and anti-homeostatic rules. Indeed, some hybrid families exhibited large  
 298 degrees of overlap between the stable regions of the network and learning rules  
 299 subsystems. However, numerical simulations revealed that these rules were mostly  
 300 ineffective in driving networks to self-sustained activity at the target setpoints  
 301 (Supplemental Material, **Section 1.2**, and Supplementary **Fig.S1**). These two results are  
 302 not inconsistent because the stability analysis speaks to cases when the network is  
 303 initialized to weights that satisfy  $E_{set}$  and  $I_{set}$ , not whether the rules will drive network  
 304 activity into these stable areas from any initial state including a pre-developmental state.  
 305 Thus, we interpret these results as meaning that while anti-homeostatic plasticity can  
 306 contribute to stability of this dual dynamical system, anti-homeostatic plasticity is  
 307 ineffective at driving the dynamics towards setpoints (in other words, that anti-  
 308 homeostatic plasticity might allow for stable Up-state but does not necessarily generate  
 309 sizable basins of attraction around Up-states).  
 310  
 311



312  
 313

314 **Figure 3. The paradoxical effect constrains the learning rules that can lead to Up-states.**

315 **(A)** Example of the self-sustained dynamics of a two-population model with weight values shown in the  
 316 diagram. Both the  $E$  and  $I$  firing rates fall below their respective setpoints. The objective is to adjust the  
 317 weights so that the  $E$  and  $I$  activity match their setpoints.

318 **(B)** An increase of  $W_{IE}$  from 10 to 12 results in a paradoxical decrease of the  $I$  rate.

319 **(C)** Because of the paradoxical effect an effective way to increase the steady-state  $I$  firing rate is to  
 320 decrease its excitatory drive (i.e.,  $W_{IE}$ ).  
 321  
 322

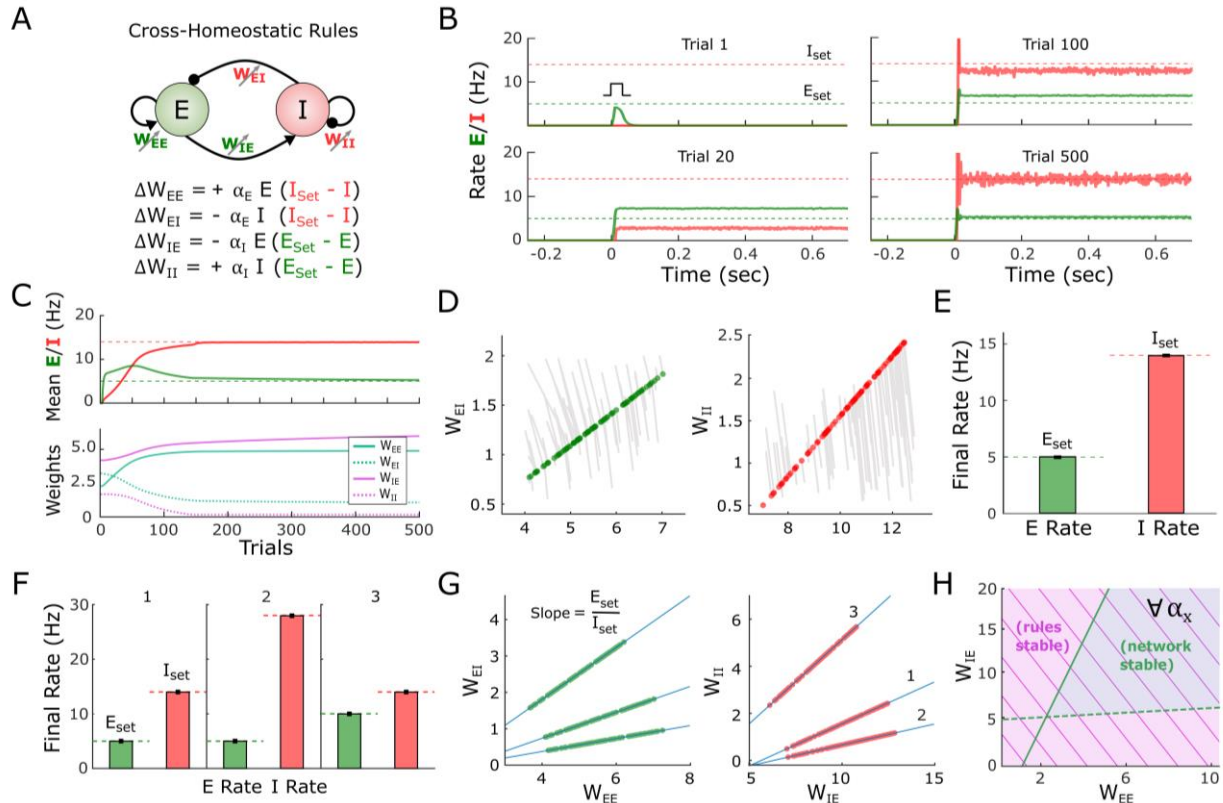
## 323 **A novel cross-homeostatic rule robustly leads to the emergence of self-sustained** 324 **Up-states**

325  
326 Given that a standard set of homeostatic learning rules did not robustly lead to self-  
327 sustained dynamics we explored alternative learning rules. By defining a loss function  
328 based on the sum of the excitatory and inhibitory errors we analytically derived a set of  
329 learning rules using gradient descent (see **Section 3** in the Supplementary Material). This  
330 approach led to mathematically complex and biologically implausible rules; however,  
331 approximations and simulations inspired a simple class of learning rules that we will refer  
332 to as cross-homeostatic (see Methods). The main characteristic of this set of rules is that  
333 the homeostatic setpoints are “crossed” (**Fig. 4A**). Specifically, the weights onto the  
334 excitatory neuron ( $W_{E \leftarrow E}$  and  $W_{E \leftarrow I}$ ) are updated to minimize the inhibitory error while  
335 weights into the inhibitory neuron ( $W_{I \leftarrow E}$  and  $W_{I \leftarrow I}$ ) change to minimize the excitatory  
336 error. Although apparently non-local, from the perspective of an excitatory neuron these  
337 rules can be interpreted as cells having a setpoints for the inhibitory input current onto the  
338 cell. Such input could be read by a cell as the activation of metabotropic receptors (e.g,  
339 GABA<sub>b</sub> and mGlu; see Discussion). Indeed, a similar cross-homeostatic rule has been  
340 derived for  $W_{I \leftarrow E}$  weights (Mackwood et al., 2021).

341  
342 An example of the performance of the cross-homeostatic rules is shown in **Fig. 4B-C**.  
343 After an initial phase with no self-sustained firing (Trial 1), recurrent activity reaches a  
344 stable Up-state (Trial 20), whose average rate continues to converge towards its defined  
345 setpoints (Trial 100) until the learning rule system reaches steady state (Trial 500). The  
346 average  $E$  and  $I$  rates of the network evolve asymptotically towards the defined setpoints,  
347 as the weights evolve and converge (**Fig. 4C**). Across different weight initializations the  
348 rules proved effective in driving the mean Up-state activity of the network to the target  $E$   
349 and  $I$  setpoints, and led to balanced dynamics (**Fig. 4D-E**). The weight trajectory from its  
350 initial value to its final one is shown for 100 different simulations (**Fig. 4D**). Each line  
351 corresponds to individual experiments with different initializations. Circles indicate the  
352 final values of the weights. Independently of the initial conditions, the weights converge  
353 to a line attractor (actually a 2D plane attractor in 4D weight space; see **Section 2.1** in  
354 the Supplementary Material). Note that this attractor refers to the sets of weights that  
355 generate Up-states where  $E$  and  $I$  activity matches  $E_{set}$  and  $I_{set}$  respectively. That is, for a  
356 given pair of setpoints ( $E_{set}$ ,  $I_{set}$ ) the final values of the weights  $W_{E \leftarrow I}$  and  $W_{I \leftarrow E}$  are linear  
357 functions of the “free” weights  $W_{E \leftarrow E}$  and  $W_{I \leftarrow I}$ , respectively. This is a direct consequence  
358 of the steady state conditions for the nontrivial fixed-point of the two-population model  
359 (Tsodyks et al., 1997; Ozeki et al., 2009; Jercog et al., 2017), where the slope of the line  
360 is defined by the setpoints  $E_{set}/I_{set}$  (see Methods). For example, to satisfy  $\frac{dE}{dt} = 0$  in the Up-  
361 state fixed point, the net excitation and inhibition must obey a specific “balance”, meaning  
362 that once  $W_{E \leftarrow E}$  or  $W_{E \leftarrow I}$  is determined, the other is analytically constrained for a given  
363 set of setpoints and parameters. Once the weights reach this specific relationship, the  $E$   
364 and  $I$  rates reach their corresponding  $E_{set}$  and  $I_{set}$  values (**Fig. 4E**). Numerical simulations  
365 confirm that the cross-homeostatic rule robustly guides Up-states to different  $E_{set}$  and  $I_{set}$   
366 setpoints (**Fig. 4F**), whose ratios define the slopes of the final relationship between the  
367 weights (**Fig. 4G**).

368





369  
370  
371 **Figure 4. A family of cross-homeostatic learning rules robustly lead to self-sustained dynamics at**  
372  **$E_{set}$  and  $I_{set}$ .**

373 (A) Schematic of the network model and the family of cross-homeostatic learning rules.  
374 (B) Example network dynamics across simulated development. The network is initialized with weights  
375 that do not lead to self-sustained dynamics in response to an external input (Trial 1, weights are  
376 initialized to  $W_{EE}=2.1$   $W_{EI}=3$   $W_{IE}=4$   $W_{II}=2$ ). By Trial 20 a stable Up-state is observed, but at firing rates  
377 far from the target setpoints (dashed lines). By Trial 500 the network has converged to an Up-state in  
378 which E and I firing rate match their respective setpoints  
379 (C) Average rate across trials (upper plot) for the excitatory and inhibitory populations for the data shown  
380 in (B). Weight dynamics (bottom plot) induced by the cross-homeostatic rules across trials for the data  
381 shown in (B)  
382 (D) Weight changes for 100 different simulations with random weight initializations (see Methods). Lines  
383 show change from initial to final (circles) weight values.  
384 (E) Average final rates for 100 independent simulations with different weight initializations shown in (D).  
385 Data represents mean  $\pm$  SEM.  
386 (F) Final rates for the excitatory and inhibitory subpopulations after learning with same starting conditions  
387 as in (D) and (E) but for different setpoints. 1:  $E_{set}=5$ ,  $I_{set}=14$ ; 2:  $E_{set}=5$ ,  $I_{set}=28$ ; 3:  $E_{set}=10$ ,  $I_{set}=14$ .  
388 Data shown in (D) and (E) corresponds to 1. Data represents mean  $\pm$  SEM.  
389 (G) Final weight values for homeostatic plasticity simulations for the three different pairs of setpoints  
390 shown in (F). Blue lines correspond to the theoretical linear relationship between the excitatory and  
391 inhibitory weights at a fixed-point obeying  $E_{set}$  and  $I_{set}$ . The slope of the line is defined by the ratio of  
392 the setpoints (see Methods).  
393 (H) Analytical stability regions of the neural subsystem and learning rule subsystem as a function of  $W_{EE}$   
394 and  $W_{IE}$ . The stability condition holds for any possible combination of learning rates (see **Section 2.4**  
395 in the Supplementary Material)

396 To further validate the effectiveness and stability of the cross-homeostatic rule we again  
397 used analytic methods to determine the eigenvalues of the 4-dimensional learning-rule  
398 dynamical system governed by the family of four cross-homeostatic rules. As above,  
399 stability is determined by the sign of the real part of the eigenvalues of the system. It can  
400 be shown (see **Section 1.3** in the Supplementary Material) that this learning rule is stable  
401 for any set of parameter values, provided that the stability conditions of the neural  
402 subsystem are satisfied (**Fig. 4H**). Therefore, it is possible to formally establish that the  
403 cross-homeostatic learning rules are inherently stable, and can robustly account for the  
404 emergence and maintenance of self-sustained inhibition-stabilized dynamics in the two-  
405 population model.

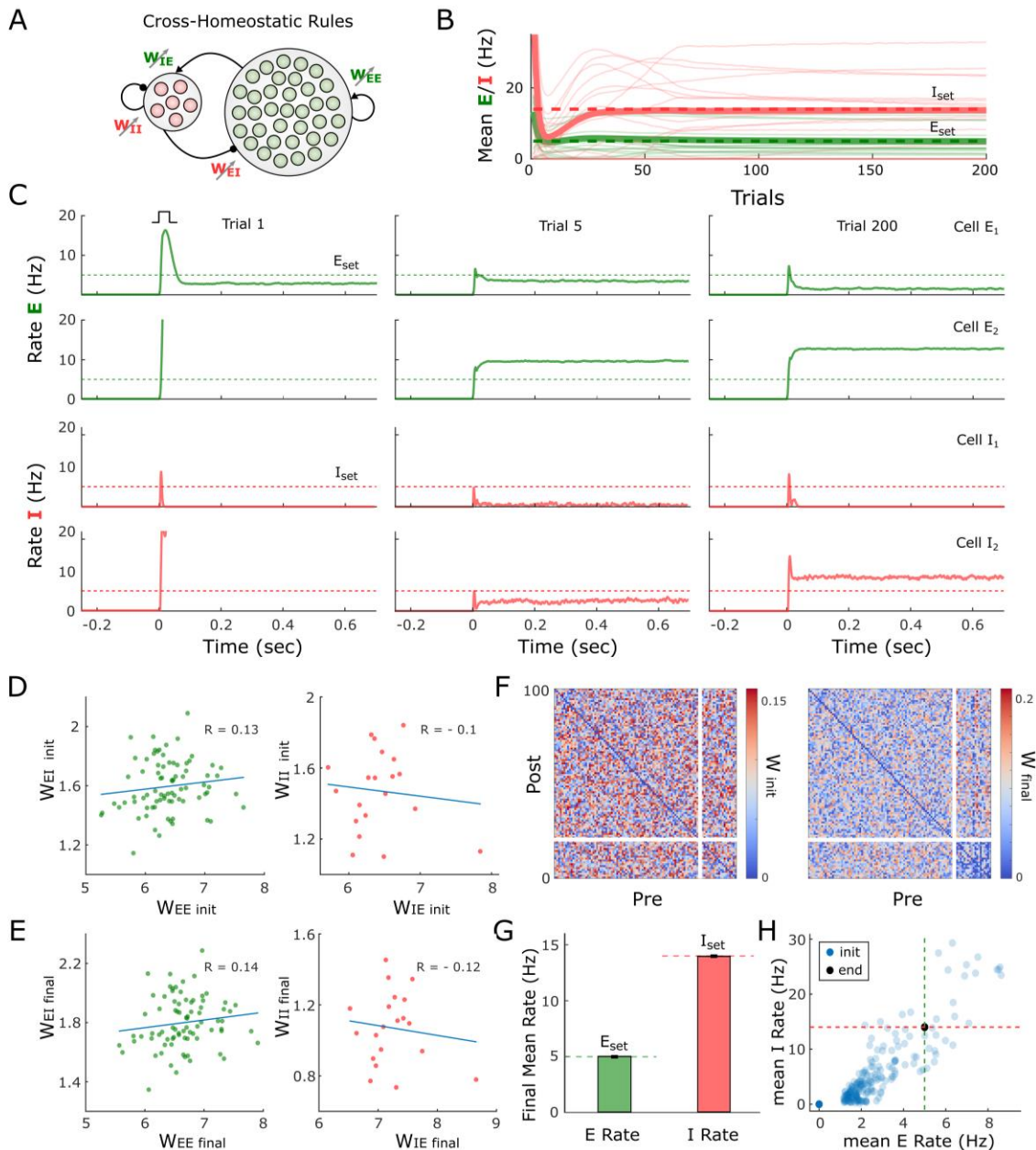
406

### 407 **Cross-homeostatic rules drive average activity in a multi-unit model to setpoints**

408

409 The previous results demonstrate the robustness of the cross-homeostatic family of rules  
410 in driving a two-subpopulation rate model to a stable Up-state. We next examined if these  
411 rules are also effective when considering a multi-unit model in which there are many  
412 excitatory and inhibitory units. The firing-rate model was composed of 80 excitatory and  
413 20 inhibitory recurrently connected neurons (**Fig. 5A**). In this case, individual neurons  
414 adjust their weights to minimize the average error of their presynaptic partners (see  
415 Methods). Starting with a random weight initialization, the network reaches stable self-  
416 sustained dynamics (**Fig. 5B-C**). However, individual units converge to different final rate  
417 values, satisfying the defined setpoints only as an average (green and red thick lines of  
418 **Fig. 5B**). This is a result of the nature of the cross-homeostatic rules: neurons adjust their  
419 weights to minimize the error of the *mean* activity of its presynaptic partners. For this  
420 reason, although the network is globally balanced, single units do not converge to the  
421 same balanced E-I line attractor (**Fig. 5D-E**), and little structure is observed in the  
422 connectivity matrix after learning (**Fig. 5F**). Simulations across 400 different initialization  
423 conditions demonstrate that the rules lead the average excitatory and inhibitory  
424 population activity to  $E_{set}$  and  $I_{set}$ , respectively (**Fig. 5G-H**). The cross-homeostatic rules  
425 are thus capable of driving a multi-unit model to a stable Up-regime, but they do not guide  
426 individual units to local setpoints.





427

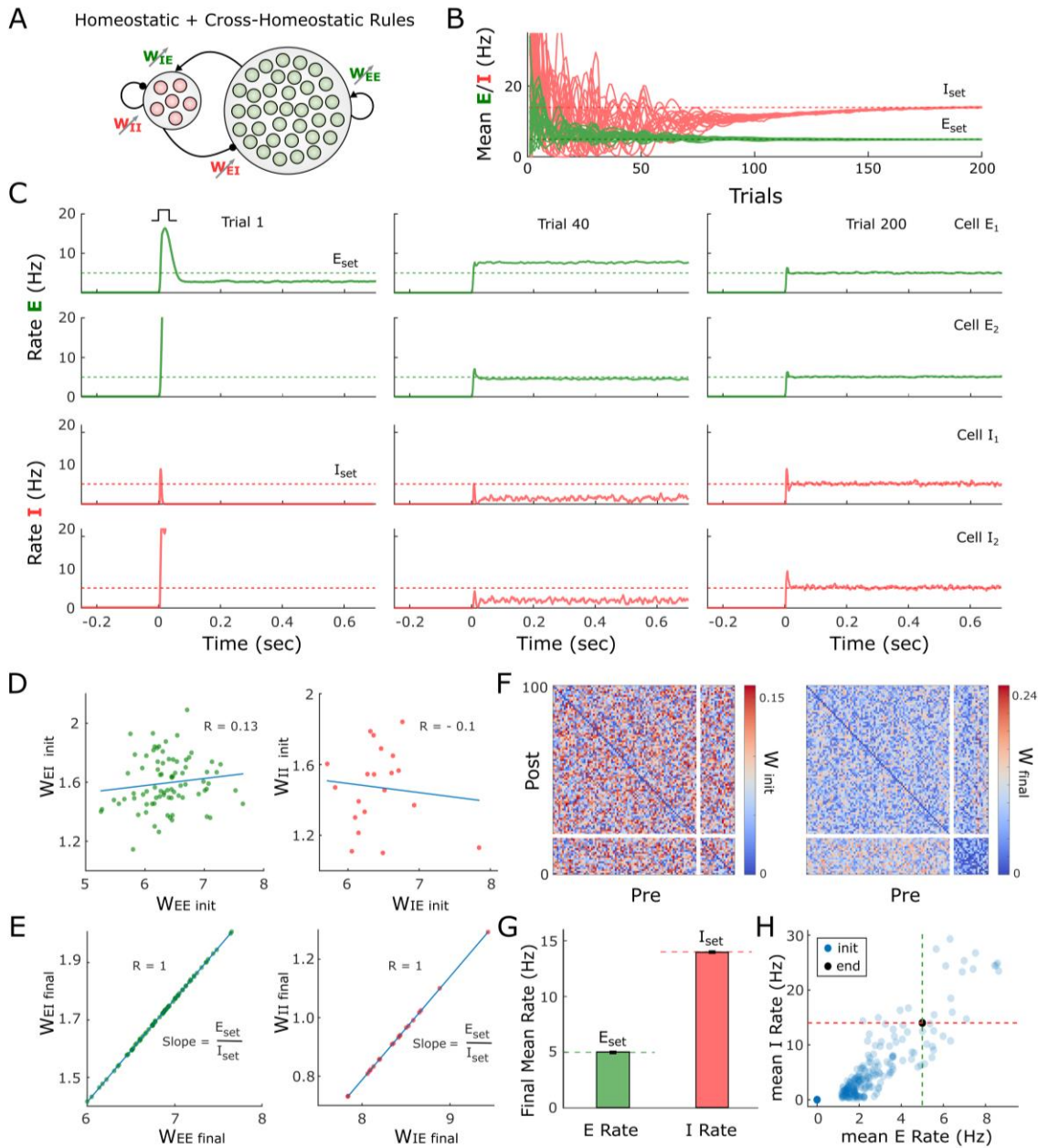
428 **Figure 5. Cross-homeostatic rules drive a multi-unit firing rate model to a global network balance.**

- 429 (A) Schematic (left) of the multi-unit rate model. The network is composed of 80 excitatory and 20 inhibitory units  
 430 recurrently connected. The four weight classes are governed by cross-homeostatic learning rules (right). See  
 431 Methods for a detailed explanation of the implementation.  
 432 (B) Evolution of the average rate across trials of 20 excitatory and inhibitory units in an example simulation. The  
 433 network is initialized with random weights (see Methods) and so neurons present diverse initial rates.  $E_{set}=5$   
 434 and  $I_{set}=14$  represent the target homeostatic setpoints. Red and green lines represent the individual (thin lines)  
 435 and average (thick lines) firing rate of inhibitory and excitatory population, respectively.  
 436 (C) Example of the firing rate of two excitatory and two inhibitory units at different points in (B). The evolution of  
 437 the firing rate of the excitatory and inhibitory population within a trial in response to a brief external input is  
 438 shown in every plot. Individual units converge to a stable Up-state but not to the defined setpoint.  
 439 (D) E-I weight relationships at the beginning of the simulation. Every dot represents the total presynaptic weight  
 440 onto a single unit. Left excitatory neurons. Right inhibitory neurons.  
 441 (E) Same plot as in D at the end of the simulation.

- 442 (F) Weight matrix for the multi-unit model at the beginning (left) and end (right) of the simulation. First 20 neurons  
443 are inhibitory.  
444 (G) Average firing rate of the units of the multi-unit model and for different initializations of weights ( $n=400$ ). The  
445 network converges to the setpoints in average. Data represents mean  $\pm$  SEM.  
446 (H) Same data as in (G) but showing the average initial rate of the network for the multiple initializations (blue  
447 dots) and the average rate at the end (black). Target rates are shown in dotted lines (green,  $E_{set}=5$ , red  $I_{set}=14$ ).  
448

## 449 **A learning rule with cross-homeostatic and homeostatic terms leads to local** 450 **convergence to setpoints.**

451  
452 The above results demonstrate a potential limitation of the cross-homeostatic family of  
453 rules: the target setpoints are only reached at the population level. An additional and  
454 potentially more serious limitation is that cross-homeostatic rules predict that artificially  
455 altering the activity of a small number of excitatory neurons within a large network would  
456 not directly produce homeostatic plasticity in these neurons, but directly produce plasticity  
457 in their postsynaptic inhibitory neurons. This prediction seems to conflict with homeostatic  
458 plasticity experiments that have targeted specific cell types rather than globally alter  
459 activity through pharmacological means (Burrone et al., 2002; Xue et al., 2014). We  
460 therefore assessed the scenario in which both cross-homeostatic and homeostatic rules  
461 operate in parallel, resulting in a “two-term cross-homeostatic” family of rules. These rules  
462 can actually be recovered after an approximation of a gradient descent derivation on a  
463 loss function that includes the difference between  $E$  and  $I$  and their respective setpoints  
464 (see **Section 3** in the Supplementary Material). In a two-subpopulation model, we first  
465 confirmed that this two-term cross-homeostatic family is stable—assuming that the  
466 learning rate of the homeostatic term does not dominate (see Supplementary Material,  
467 **Section 1.4**). Simulations with the same multi-unit model as **Fig. 5** show that with the  
468 two-term cross-homeostatic rule all individual units converge to their respective  $E_{set}$  and  
469  $I_{set}$  (**Fig. 6A-C**). Importantly, in contrast to the single-term cross-homeostatic rule the total  
470 excitatory and inhibitory weight of each individual unit converged to the E-I balance of the  
471 line attractor predicted by the network equations (**Fig. 6D-E**), while more structure is also  
472 observed in the weight matrices (**Fig. 6F**)—i.e., there is less homogeneity between the  
473 four synapse classes. The convergence to the setpoints was stable across a wide range  
474 of initial states (**Fig. 6G-H**). Thus, a hybrid family of learning rules that includes both cross-  
475 homeostatic and homeostatic forces provide global network stability, while also locally  
476 driving each unit to their setpoint and a balanced E-I regime.



477

478 **Figure 6. Adding cross-homeostatic influences to homeostatic rules lead global and local convergence to**  
 479 **setpoints.**

- 480 (A) Schematic (left) of the multi-unit rate model. The network is composed of 80 excitatory and 20 inhibitory units  
 481 recurrently connected. The four weight classes are governed by homeostatic rules with cross-homeostatic  
 482 influences (right). See Methods for a detailed explanation of the implementation.
- 483 (B) Evolution of the average rate across trials in an example simulation (20 excitatory and inhibitory units). The  
 484 network is initialized with random weights (same as in Fig. 5, see Methods) and so neurons present diverse  
 485 initial rates.  $E_{set}=5$  and  $I_{set}=14$  Hz represent the target homeostatic setpoints.
- 486 (C) Example of the firing rate of two excitatory and two inhibitory units at different points in (B). The evolution of  
 487 the firing rate of the excitatory and inhibitory population within a trial in response to a brief external input is  
 488 shown in every plot. Units converge to a stable Up-state and at an individual setpoint.
- 489 (D) E-I weight relationships at the beginning of the simulation. Every dot represents the total presynaptic weight  
 490 onto a single unit. Left excitatory neurons. Right inhibitory neurons.

- 491 (E) Same plot as in D at the end of the simulation. The network has reached a stable state and weights converge  
492 to single E-I balance defined by a line attractor.  
493 (F) Weight matrix for the multi-unit model at the beginning (left) and end (right) of the simulation. First 20 neurons  
494 are inhibitory.  
495 (G) Average firing rate of the units of the multi-unit model and for different initializations of weights (n=400). Data  
496 represents mean  $\pm$  SEM.  
497 (H) Same data as in (G) but showing the average initial rate of the network for the multiple initializations (blue  
498 dots) and the average rate at the end (overlapping black circles). Target rates are shown in dotted lines (green,  
499  $E_{set}$ , red,  $I_{set}$ ).  
500

## 501 DISCUSSION

502 Elucidating the learning rules that govern the connectivity within neural circuits  
503 represents a fundamental goal in neuroscience, in part, because learning rules establish  
504 unifying principles that span molecular, cellular, systems, and computational levels of  
505 analyses. Elucidation of Hebbian associative synaptic plasticity, for example, linked  
506 simple computations at the level of single proteins (the NMDA receptor) with higher-order  
507 computations at the systems and computational levels (Hebb, 1949; Miller et al., 1989;  
508 Buonomano and Merzenich, 1998; Martin et al., 2000; Song et al., 2000). However, it  
509 remains the case that relatively little is known about the learning rules that give rise to  
510 complex neural dynamic regimes. Here we have taken steps towards exploring families  
511 of learning rules that operate in parallel at four different synapse classes and capture the  
512 experimentally observed emergence of Up-states in cortical networks.

513  
514 Towards this goal we first confirmed that, in agreement with previous studies (Johnson  
515 and Buonomano, 2007; Motanis and Buonomano, 2020), Up-states emerge over the  
516 course of weeks of *ex-vivo* development. Because cortical organotypic cultures maintain  
517 much of their local and laminar architecture, and are mostly isolated from other cortical  
518 and subcortical inter-areal connectivity (Bolz, 1994; Echevarria and Albus, 2000; De  
519 Simoni et al., 2003), these results suggest the presence of local learning rules that lead  
520 to self-sustained, inhibition-stabilized activity in the absence of any supervisory,  
521 modulatory, or structured input signals from other brain areas.

522  
523 We first explored whether standard formulations of homeostatic plasticity can account  
524 for the unsupervised emergence of Up-states—or more generally of self-sustained,  
525 inhibition-stabilized regimes. Based on experimental data we assumed that both  
526 excitatory and inhibitory neurons have an ontogenetically programmed activity setpoint  
527 during Up-states and that plasticity at the four weight classes is driven by homeostatic  
528 plasticity. Numerical simulations and analytical stability analyses revealed that while  
529 some initial conditions and parameter regimes led to self-sustained dynamics, they  
530 occupied a relatively narrow region of parameter space: when the rate of synaptic  
531 plasticity onto inhibitory neurons is much lower than that onto excitatory neurons (**Fig. 2**,  
532 and Supplementary Materials). When the rate of inhibitory and excitatory plasticity are  
533 comparable, analytical stability analyses confirmed that the region of stability of the  
534 network dynamics only overlapped in a narrow region. Such a narrow stability area seems  
535 incompatible with the robustness necessary in biological systems, and with experimental  
536 data showing that inhibitory neurons exhibit as much or more homeostatic plasticity than  
537 excitatory neurons (Keck et al., 2011; Kuhlman et al., 2013; Gainey et al., 2018; Ma et



538 al., 2019). We thus conclude that a family of standard homeostatic learning rules  
539 operating at all four synapse classes is not sufficient to account for the experimentally  
540 observed emergence of self-sustained dynamics in cortical circuits.

541

## 542 **Cross-homeostatic plasticity**

543

544 Analyses of approximations of a gradient-descent-derived learning rule suggested,  
545 somewhat counterintuitively, that adjusting the  $E$  population based on the error of the  $I$   
546 population (and vice-versa) may prove to be an effective family of learning rules. Indeed,  
547 numerical simulations and analytical stability analyses revealed that this cross-  
548 homeostatic rule was robustly stable (**Fig. 4**). The convergence to the excitatory and  
549 inhibitory setpoints, however, only occurred at the population level, not at the level of  
550 individual units. This observation, however, is not inconsistent with experimental data,  
551 which shows that *in vivo* neurons do exhibit a wide range of variability in their apparent  
552 setpoints (Hengen et al., 2016; Trojanowski et al., 2020). However, a significant concern  
553 with this single-term cross-homeostatic rule is that it predicts that selectively increasing  
554 activity in a subpopulation of excitatory neurons would first induce plasticity in inhibitory  
555 neurons ( $W_{I \leftarrow E}$  and  $W_{I \leftarrow I}$ )—which could in turn lead to plasticity in the manipulated  
556 excitatory neurons ( $W_{E \leftarrow E}$  and  $W_{E \leftarrow I}$ ). Most homeostatic plasticity studies do not speak  
557 to this prediction because they have used pharmacological manipulations of both  
558 excitatory and inhibitory neurons. However, some studies have used cell-specific  
559 manipulations—e.g., cell-specific overexpression of potassium channels (Burrone et al.,  
560 2002; Xue et al., 2014)—that strongly support the notion that synaptic plasticity is guided  
561 at least in part on their own deviation from setpoint.

562

563 In our opinion, and although we have explored alternative rules (see Supplementary  
564 Material, **Section 1.6**), the most biologically plausible set of learning rules that lead to  
565 stable Up-states comprises a hybrid rule that includes both standard homeostatic and  
566 cross-homeostatic terms. Such a two-term cross-homeostatic rule robustly led to a self-  
567 sustained, inhibition-stabilized network, led to all units converging to their setpoints, and  
568 is directly consistent with current experimental data.

569

## 570 **Biological plausibility of cross-homeostatic plasticity**

571

572 While the neural mechanisms underlying homeostatic plasticity remain to be  
573 elucidated, it is generally assumed that an individual neuron can maintain a running  
574 average of their firing rate over the course of hours as a result of  $Ca^{2+}$ -activated sensors.  
575 Based on the deviation of this value from an ontogenetically determined setpoint, neurons  
576 up- or down-regulate the density of postsynaptic receptors accordingly (Liu et al., 1998;  
577 Joseph and Turrigiano, 2017; Trojanowski et al., 2020). Two-term cross-homeostatic  
578 plasticity would require an additional, and apparently non-local information about the error  
579 in a given neuron's presynaptic partners. It is important to stress, however, that this rule  
580 is not necessarily a non-local rule, because any postsynaptic neuron has access to the  
581 mean activity of its presynaptic partners simply as a result of its postsynaptic receptor  
582 activation. Indeed, a plasticity rule for  $W_{I \leftarrow E}$  weights with a similar cross-homeostatic error  
583 term has also been recently proposed and implemented based on the mean activation of

584 postsynaptic receptors—more specifically the net postsynaptic currents which provide a  
585 coupled measure of average presynaptic firing and synaptic weights (Mackwood et al.,  
586 2021).

587  
588 Here we propose that cross-homeostatic plasticity could be implemented through  
589 metabotropic postsynaptic metabotropic receptors—e.g., mGlu and GABA<sub>b</sub>. Such  
590 receptors would provide a mechanism for postsynaptic neurons to maintain a running  
591 average of the activity of its presynaptic partners that is decoupled from the synaptic  
592 weights. Metabotropic receptors are G-protein coupled receptors (GPCR) that provide a  
593 low-pass filtered measure of presynaptic activity and are involved in a large number of  
594 incompletely understood neuromodulatory roles (Blein et al., 2000; Niswender and Conn,  
595 2010). Since metabotropic receptors appear to undergo less homeostatic and associative  
596 plasticity, they provide a measure of presynaptic activity that is naturally decoupled from  
597 the ionotropic receptors (e.g., AMPA and GABA<sub>a</sub>) that are being up- and down-regulated.  
598

599 Further support for the notion that individual neurons have access to global network  
600 activity emerges from studies suggesting that neurons might not homeostatically regulate  
601 activity at the individual neuron level, but rather at the global population level (Slomowitz  
602 et al., 2015). Such a global-level homeostasis could be achieved by non-synaptic  
603 paracrine transmission. Indeed, retrograde messenger systems are ideally suited for this  
604 role, as they have already been implicated in signaling mean activity levels to local  
605 capillaries, driving the activity-dependent vasodilation that underlies fMRI (Drew, 2019).  
606

### 607 **The paradoxical effect and standard homeostatic rules**

608  
609 The paradoxical effect is one of the defining features of inhibition-stabilized networks,  
610 and a growing body of evidence suggests that Up-states and other self-sustained  
611 dynamic regimes are instantiations of inhibition-stabilized networks (Zucca et al., 2017;  
612 Mahrach et al., 2020; Sanzeni et al., 2020; Sadeh and Clopath, 2021). Here we show that  
613 the paradoxical effect applies important constraints to the potential learning rules that lead  
614 to the emergence of inhibition-stabilized networks. In the simplified case in which there is  
615 only homeostatic plasticity onto the inhibitory neurons, we can immediately see why the  
616 paradoxical effect renders standard homeostatic rules ineffective. If the  $I$  population is  
617 below its setpoint, the standard homeostatic rules would increase  $W_{I \leftarrow E}$ , which  
618 paradoxically would further decrease  $I$  (**Fig. 3**), thus further increasing the error instead  
619 of decreasing it (**Fig. 3**). This reasoning is related to why, when using the standard family  
620 of homeostatic rules, the rate of plasticity onto the inhibitory neurons has to be much  
621 smaller—in effect dampening the “paradoxical homeostatic plasticity effect”. Furthermore,  
622 our analytical stability analyses show that in the limit of vanishingly small excitatory  
623 learning rates ( $\alpha_{EE,EI} \ll \alpha_{IE,II}$ ) the stability region of the weight subsystem is bounded by  
624 the paradoxical condition. This means that the only allowed stable states with non-zero  $E$   
625 activity will occur in the non-paradoxical regime, if any, and they will not be proper  
626 inhibition-stabilized Up-states.  
627



## 628 **Future directions and experimental predictions**

629

630 While we implemented homeostatic learning rules at all four synapses classes in our  
631 model, it is important to stress that we have omitted other well-characterized forms of  
632 synaptic plasticity. Of particular relevance, we did not include associative LTP or STDP.  
633 These forms of plasticity are generally considered to capture the correlation structure in  
634 networks which are driven by structured inputs. Arguably, because our circuits develop in  
635 the absence of any structured external input and because all excitatory and inhibitory  
636 neurons synchronously shift between Down $\leftrightarrow$ Up states, it is possible that associative  
637 forms of plasticity do not contribute significantly to Up-state development. Nevertheless,  
638 future experimental and theoretical studies have to address the potential role for  
639 associative forms of synaptic plasticity in Up-state development.

640

641 An important implication of our results is that neuronal and network properties can  
642 operate in fundamentally different ways. That is, while homeostatic plasticity can lead to  
643 single neurons to reach their target setpoints in simple feedforward circuits, those same  
644 rules can be highly unstable when the neurons are placed even in the simplest of  
645 recurrent excitatory/inhibitory circuits with emergent dynamics. Furthermore, because  
646 emergent neural dynamic regimes are highly nonlinear, and in particular, that stable self-  
647 sustained dynamic regimes exhibit a paradoxical effect, it is likely that the brain exhibits  
648 “paradoxical” or counterintuitive learning rules to generate self-sustained dynamic  
649 regimes.

## 650 METHODS

651

### 652 *Ex vivo slice preparation*

653 Organotypic slices were prepared using the interface method (Stoppini et al., 1991; Goel  
654 and Buonomano, 2016). Briefly, five to seven day-old WT and PV-Cre mice were  
655 anesthetized with isoflurane and decapitated. The brain was removed and placed in  
656 chilled cutting media. Coronal slices (400  $\mu\text{m}$  thickness) containing auditory cortex were  
657 sliced using a vibratome (Leica VT1200) and placed on filters (MillicellCM, Millipore,  
658 Billerica, MA, USA) with 1 mL of culture media. Culture media was changed at 1 and 24  
659 hours after cutting and every 2-3 days thereafter. Cutting media consisted of EMEM  
660 (MediaTech cat. #15-010) plus (final concentration in mM):  $\text{MgCl}_2$ , 3; glucose, 10;  
661 HEPES, 25; and Tris-base, 10. Culture media consisted of EMEM plus (final  
662 concentration in mM): glutamine, 1;  $\text{CaCl}_2$ , 2.6;  $\text{MgSO}_4$ , 2.6; glucose, 30; HEPES, 30;  
663 ascorbic acid, 0.5; 20% horse serum, 10 units/L penicillin, and 10  $\mu\text{g/L}$  streptomycin.  
664 Slices were incubated in 5%  $\text{CO}_2$  at 35°C.

665

### 666 *Two-photon Calcium Imaging*

667 Organotypic slices from PV-Cre mice (Jackson Laboratory #017320) were transfected at  
668 1-3 DIV with pENN-AAV-CaMKII-GCaMP6f-WPRE-SV40 to selectively express  
669 GCaMP6f in excitatory neurons, and pAAV-CAG-Flex-mRuby2-GSG-P2A-GCaMP6f-  
670 WPRE-pA to visualize and selectively express GCaMP6f in PV<sup>+</sup> inhibitory neurons.  
671 Transfection was achieved by gently delivering 1 $\mu\text{L}$  of each virus onto the slice using a  
672 micropipette. Experiments were performed at least 12 days after transfection to allow for  
673 robust expression.

674

675 Calcium imaging was performed with a galvo-resonant-scanning two-photon  
676 microscope (Neurolabware) controlled by Scanbox acquisition software  
677 (<https://scanbox.org>). A Coherent Chameleon Ultra II Ti:sapphire laser (Cambridge  
678 Technologies) was used for GCaMP6f (920 nm) and mRuby excitation (1040 nm). A  
679 16x water-immersion lens (Nikon, 0.8 NA, 3 mm working distance) was used. Image  
680 sequences were captured using unidirectional scanning at a frame rate of  $\sim 15$  Hz. The  
681 size of the recorded imaging field was  $\sim 520 \times 800 \mu\text{m}$  ( $512 \times 796$  pixels). Five min of  
682 spontaneous activity was recorded at 920 nm at every developmental time point. Before  
683 the recording a snapshot at 1040 nm was recorded in order to identify PV<sup>+</sup> neurons.  
684 Regions of interests (ROI) for both excitatory and PV<sup>+</sup> neurons were established using  
685 the imaging processing pipeline Suite2p (<https://github.com/MouseLand/suite2p>)  
686 (Pachitariu et al., 2017).  $\Delta F/F$  was calculated as  $(F(t) - F_0)/F_0$ , where  $F(t)$  was the raw  
687 fluorescence filtered with a median filter with a window of 1 s.  $F_0$  was the running median  
688  $F(t)$  over the previous 20 s window. For each recorded slice and neural population  
689 (excitatory or PV<sup>+</sup>), potential Up-states were identified based on a threshold set at 1 above  
690 the mean z-scored raw fluorescence  $F$  trace of all neurons. If these events remained  
691 above threshold for at least one second, they were classified as Up-states. Mean Up

692 Frequency and Duration were computed over all Up-states detected within the 5 min  
693 spontaneous activity period.

694

### 695 **Computational model**

696 A two-population firing-rate model was implemented based on Jercog et al (2017). The  
697 firing rate of the excitatory ( $E$ ) and inhibitory ( $I$ ) population obeyed Wilson and Cowan  
698 dynamics (Wilson and Cowan, 1972):

699

$$700 \quad (1) \quad \tau_E \frac{dE}{dt} = -E + f_E(W_{EE}E(t) - W_{EI}I(t) - a + \eta_E(t))$$

$$701 \quad (2) \quad \tau_I \frac{dI}{dt} = -I + f_I(W_{IE}E(t) - W_{II}I(t) + \eta_E(t))$$

702

703 where  $W_{XY}$  represents the weight between the presynaptic unit  $Y$  and postsynaptic unit  
704  $X$ .  $\tau_X$  and  $\eta_X$  represent a time constant and an independent noise term, respectively. The  
705 time constants were set to  $\tau_E = 10ms$  for the excitatory and  $\tau_I = 2ms$  for the inhibitory  
706 subpopulations. The noise term was an Ornstein-Uhlenbeck process with mean  $\mu_x = 0$ , a  
707 time constant  $1/\theta_x = 1ms$ , and a sigma parameter of  $\sigma_x = 10$ . To elicit Up-states a step  
708 current was injected at the beginning of each trial on the excitatory population.

709

710 The function  $f_Y(x)$  represents the intrinsic excitability of the neurons, and it is modeled  
711 as a threshold-linear (ReLU) function with threshold  $\theta_Y$  and gain  $g_Y$ .

712

$$713 \quad (3) \quad f_Y(x) = \begin{cases} 0 & \text{if } x < \theta_Y \\ g_Y(x - \theta_Y) & \text{if } x \geq \theta_Y \end{cases}, Y = \{E, I\}$$

714

715 As in Jercog et al (2017) the thresholds were set to  $\theta_E = 4.8$  and  $\theta_I = 25$ , and the gains to  
716  $g_E = 1$  and  $g_I = 4$ . The higher thresholds in PV neurons are consistent with experimental  
717 findings (Romero-Sosa et al., 2021).

718

719 The linear relationship between excitatory and inhibitory weights (**Fig. 4**) correspond  
720 to the steady-state solution of the neural subsystem when the inhibitory and excitatory  
721 rates are at its target setpoints. The solution can be obtained by setting the left side of  
722 equations (1) and (2) to zero, and substituting the steady state  $E$  and  $I$  values by  $E_{Set}$  and  
723  $I_{Set}$ .

724

$$725 \quad (4) \quad W_{EI} = \frac{W_{EE}E_{Set}}{I_{Set}} - \frac{\theta_E g_E + E_{Set}}{I_{Set} g_E}$$

726

$$727 \quad (5) \quad W_{II} = \frac{W_{IE}E_{Set}}{I_{Set}} - \frac{\theta_I g_I + I_{Set}}{I_{Set} g_I}$$

728

729 Thus, the slope of the E/I balance line in **Fig. 4** corresponds to  $E_{Set}/I_{Set}$ . See details and  
730 analytical results in **Section 2.2** of the Supplementary Material.

731

## 732 **Synaptic plasticity**

733 Plasticity at all four weight classes ( $W_{E \leftarrow E}$ ,  $W_{E \leftarrow I}$ ,  $W_{I \leftarrow E}$ ,  $W_{I \leftarrow I}$ ) was governed by different  
734 families of homeostatic based learning rules, all driven by the deviation of the actual  
735 excitatory and inhibitory rates from their target setpoints ( $E_{set}$  and  $I_{set}$ ). Three different  
736 learning rules are presented in the main text of this paper.

737

738 *Standard homeostatic family of rules:*

739

$$\begin{aligned} 740 \quad (6) \quad \Delta W_{EE} &= +\alpha_E E (E_{set} - E) \\ 741 \quad \Delta W_{EI} &= -\alpha_E I (E_{set} - E) \\ 742 \quad \Delta W_{IE} &= +\alpha_I E (I_{set} - I) \\ 743 \quad \Delta W_{II} &= -\alpha_I I (I_{set} - I) \end{aligned}$$

744

745 where  $\alpha_E$  and  $\alpha_I$  are the learning rates onto the excitatory and inhibitory units,  
746 respectively. All alphas are set to equal values in the simulation data shown in **Fig. 2** ( $\alpha =$   
747 0.0001). The setpoints were based on empirically measured values in *ex vivo* cortical  
748 circuits (Romero-Sosa et al., 2021):  $E_{set} = 5$  and  $I_{set} = 14$  Hz.

749

750 The configuration of setpoints follows a classic homeostatic formulation (Turrigiano et  
751 al., 1998; Rossum et al., 2000; Liu and Buonomano, 2009; Vogels et al., 2011), where  
752 every neural population adapts its input weights homeostatically in order to minimize its  
753 error term. As outlined in Supplementary Material (**Section 1.5**) we also examined  
754 variants of this formulation, such as standard synaptic scaling (which includes the weight  
755 as factor).

756

757 We prove that these rules are only stable in a narrow parameter regime (when excitatory  
758 plasticity dominates). See details and analytical results in **Section 2** of the Supplementary  
759 Material.

760

761 *Single-term cross-homeostatic family of rules:*

762

$$\begin{aligned} 763 \quad (7) \quad \Delta W_{EE} &= +\alpha_E E (I_{set} - I) \\ 764 \quad \Delta W_{EI} &= -\alpha_E I (I_{set} - I) \\ 765 \quad \Delta W_{IE} &= -\alpha_I E (E_{set} - E) \\ 766 \quad \Delta W_{II} &= +\alpha_I I (E_{set} - E) \end{aligned}$$

767

768 All alphas are set to equal values in the simulation data shown in **Fig. 4** ( $\alpha = 0.0001$ ),  
769 except on the example shown in **Fig. 4B-C**, where a rate of  $\alpha = 0.0005$  was used. We note  
770 that an equivalent rule for  $W_{IE}$  has been recently derived (Mackwood et al., 2020). For  
771 **Fig. 4** two alternative pairs of setpoints were explored ( $E_{set} = 5$  and  $I_{set} = 24$ ) and ( $E_{set} =$   
772 10 and  $I_{set} = 14$ ).

773

774 We prove that these rules are stable for any set of parameters. See details and analytical  
775 results in **Section 1.3** of the Supplementary Material.

776

777

778 *Two-term cross-homeostatic family of rules:*

779

$$(8) \quad \begin{aligned} \Delta W_{EE} &= +\alpha_E E(E_{set} - E) + \alpha_E E(I_{set} - I) \\ \Delta W_{EI} &= -\alpha_E I(E_{set} - E) - \alpha_E I(I_{set} - I) \\ \Delta W_{IE} &= +\alpha_I E(I_{set} - I) - \alpha_I E(E_{set} - E) \\ \Delta W_{II} &= -\alpha_I I(I_{set} - I) + \alpha_I I(E_{set} - E) \end{aligned}$$

784

785 A single shared learning rate ( $\alpha = 0.00001$ ) was used for **Fig. 6** (see section below on the  
786 multi-unit model). We prove that these rules are stable for a biologically meaningful set of  
787 parameter values, as long as the homeostatic part does not dominate (Supplementary  
788 Material, **Section 1.4**). The two-term rules combine homeostatic and cross-homeostatic  
789 terms. This formulation can be obtained after an approximation of a gradient descent  
790 derivation on the following loss function:

791

$$(9) \quad L = \frac{1}{2}(E - E_{set})^2 + \frac{1}{2}(I - I_{set})^2$$

793

794 The mathematical derivation can be found in the Supplementary Material (**Section 3**).

795

796 An additional *Forced-Balance* learning rule, which exploits the steady-state solution of the  
797 neural subsystem at its target setpoints (equations 5 and 6), has also been explored (see  
798 **Section 1.6** of the Supplementary Material).

799

800 *All rules, numerical simulations:*

801 For all simulations, the weights were updated after the completion of every trial. The trials  
802 lasted 2 seconds. For our numerical simulations,  $E$  and  $I$  on every rule are implemented  
803 as average firing rates. The average of  $E$  and  $I$  is computed after every trial and then is  
804 low pass filtered by a process with a time constant  $\tau_{trial} = 2$ . The numerical integration  
805 time step was 0.1 ms. A minimum weight of 0.1 was set for all weights.

806

807 A saturation to the excitatory and inhibitory firing rate (100 and 250 Hz, respectively)  
808 was added to prevent the nonbiological scenario in which activity could diverge towards  
809 infinity under unstable conditions. Note the saturation is not necessary for the cross-  
810 homeostatic rule because it is inherently stable as proved in the Supplementary Material  
811 (**Section 1.3**).

812

813 In **Fig. 2D** and **4D-G** we initialize the weights uniformly in between the following  
814 ranges:  $W_{EE}[4,7]$ ,  $W_{EI}[0.5,2]$ ,  $W_{IE}[7,13]$ ,  $W_{II}[0.5,2]$ . Simulations were run for 3000 trials to  
815 assess stability and convergence.

816

817 *All rules, analytical stability analyses:*

818 We analyzed the entire dynamical system (composed of the neural subsystem and  
819 learning rule subsystem) for every synaptic learning rule considered in this work, and  
820 analyzed its stability. In every case, the general prescription is:

- 821 a) Take the combined neural and learning rule subsystems and nondimensionalize  
822 all variables, so that the two different time scales are evident (fast neural, slow  
823 synaptic plasticity). For the description of the learning rule subsystem we switch  
824 from discrete-time dynamics to continuous-time dynamics:  $\Delta W \rightarrow \tau_0 dW/dt$
- 825 b) Make a quasi-steady state (QSS) approximation of the neural subsystem. This  
826 means we will consider the neural subsystem is fast enough so that it converges  
827 “instantaneously” (when compared to the synaptic plasticity subsystem) to its  
828 corresponding fixed point. For this we will require that the stability conditions of the  
829 neural subsystem are satisfied (see below).
- 830 c) Find the steady-state solution of the synaptic plasticity subsystem, i.e. the Up-state  
831 fixed point; compute the Jacobian of the synaptic plasticity subsystem at the Up-  
832 state; compute the eigenvalues of the Jacobian. Two out of the four eigenvalues  
833 are expected to be zero because the Up-state is not an isolated fixed point of the  
834 system but a continuous 2D plane in 4D weight space.
- 835 d) Address (linear) stability. If both nonzero eigenvalues have negative real parts,  
836 then the Up-state is stable under the learning rule; if at least one of the nonzero  
837 eigenvalues has positive real part, then the Up-state is unstable. (A note on abuse  
838 of notation: we might say indistinctly “the Up-state is stable/unstable” and “the  
839 learning rule is stable/unstable”.)

840

841 See **Section 2** in the Supplementary Material.

842

### 843 ***Multi-unit firing rate model***

844 A rate-based recurrent network model containing  $N_e = 80$  excitatory and  $N_i = 20$  inhibitory  
845 neurons was implemented with all-to-all connectivity (without self-connections). The  
846 activation of the neurons followed equations (1), (2) and (4). The same parameters as for  
847 the population model were used, where  $W_{XY}$  represents now a matrix of synaptic weights  
848 from population  $X$  to population  $Y$ . A minimum weight of  $0.1/N_x$  for  $W_{EI}$  and  $W_{IE}$  and  
849  $0.1/(N_x-1)$  for  $W_{EE}$  and  $W_{II}$  was set for all weights.

850

851 The synaptic plasticity rules were implemented as follows.

852

853 *Cross-homeostatic family of rules:*

854

855

$$(10) \quad \Delta W_{ij}^{EE} = +\alpha E_j \sum_{k=1}^{N_I} (I_{set} - I_k) / N_I$$



$$\begin{aligned}
 856 \quad \Delta W_{ij}^{EI} &= -\alpha I_j \sum_{k=1}^{N_I} (I_{set} - I_k) / N_I \\
 857 \quad \Delta W_{ij}^{IE} &= -\alpha E_j \sum_{k=1}^{N_E} (E_{set} - E_k) / N_E \\
 858 \quad \Delta W_{ij}^{II} &= +\alpha I_j \sum_{k=1}^{N_E} (E_{set} - E_k) / N_E
 \end{aligned}$$

859  
860  
861 Where  $i$  and  $j$  represent the post- and presynaptic neurons, respectively, and  $k$  denotes  
862 the presynaptic inhibitory neurons targeting the excitatory neurons (or the presynaptic  
863 excitatory neurons targeting an inhibitory neuron).  $N_E$  and  $N_I$  denote the total number of  
864 excitatory and inhibitory neurons, respectively. The weights are therefore updated  
865 following the *average* presynaptic error of the crossed E/I population classes. Note as  
866 stated above that this formulation can be implemented in a local manner (see Discussion).  
867 A learning rate of  $\alpha = 0.00002$  was used for all simulations.

868  
869 *Two-term cross-homeostatic family of rules:*

$$\begin{aligned}
 870 \quad (11) \quad \Delta W_{ij}^{EE} &= +\alpha E_j (E_{set} - E_i) + \alpha E_j \sum_{k=1}^{N_I} (I_{set} - I_k) / N_I \\
 871 \quad \Delta W_{ij}^{EI} &= -\alpha I_j (E_{set} - E_i) - \alpha I_j \sum_{k=1}^{N_I} (I_{set} - I_k) / N_I \\
 872 \quad \Delta W_{ij}^{IE} &= +\alpha E_j (I_{set} - I_i) - \alpha E_j \sum_{k=1}^{N_E} (E_{set} - E_k) / N_E \\
 873 \quad \Delta W_{ij}^{II} &= -\alpha I_j (I_{set} - I_i) + \alpha I_j \sum_{k=1}^{N_E} (E_{set} - E_k) / N_E
 \end{aligned}$$

874  
875 Here the first term represents the standard homeostatic rule, and the second term cross-  
876 homeostatic plasticity (as implemented above). A learning rate of  $\alpha = 0.00001$  was used  
877 for all simulations.

878  
879 In **Fig. 5G-H** and **6G-H** we initialize the mean weights of the population uniformly in  
880 between the following ranges:  $W_{EE}[1,6]$ ,  $W_{EI}[0.5,2]$ ,  $W_{IE}[5,7]$ ,  $W_{II}[0.5,2]$ . The weights

881 within each class were normally distributed around that mean (normalized by the  
882 number of neurons) with a variance of 0.1. Note that this initialization led to multiple initial  
883 conditions with exploding network rates (which were held in check by the saturation  
884 cutoff). Those initial rates are not displayed in **Fig. 5-6H** for visualization purposes, but  
885 the rules successfully brought all those cases to the corresponding setpoints. Simulations  
886 were run for 1000 trials to assess stability of the convergence. In the example shown in  
887 **Fig. 5A-F** and **6A-F** the weights were initialized uniformly in the interval [0 0.16] and the  
888 simulation was run for 200 trials.

889

### 890 ***Statistics and Software availability***

891 Data are represented by the mean  $\pm$  SEM. In **Fig. 1** a two-way ANOVA was performed to  
892 assess interaction of time and group (cell-type) on the development of Up-states.

893

894 Experimental and computational analysis were performed in custom-written MATLAB  
895 R2020a software. SageMath was used for the analytical proofs (see Supplementary  
896 Material). The MATLAB source code that reproduces **Fig. 2, 4, 5** and **6** is available at  
897 <https://github.com/saraysoldado/UpDev2021>. The Jupyter notebooks with SageMath  
898 code to reproduce all analytical results are available at:  
899 <https://github.com/SMDynamicsLab/UpDev2021>.

900

## SUPPLEMENTARY FIGURES

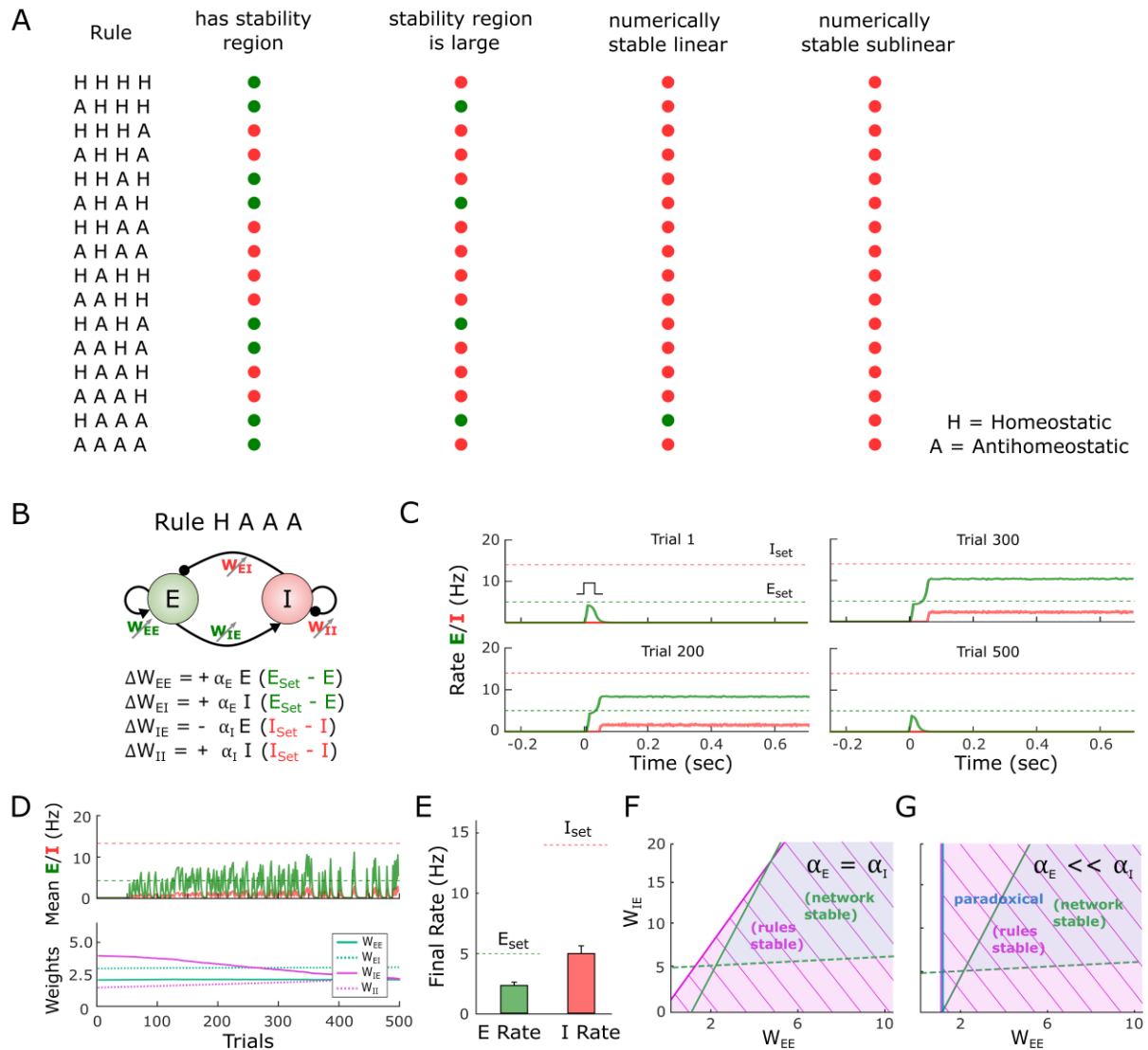


**Figure S1. Homeostatic and anti-homeostatic combinations of learning rules also fail to generate the emergence of self-sustained dynamics.**

**(A)** Sixteen variations of the standard homeostatic rules presented in **Fig. 2** were assessed for stability. The learning governing each four weight types,  $W_{EE}$ ,  $W_{EI}$ ,  $W_{IE}$ ,  $W_{II}$  was set to be either homeostatic (H) or antihomeostatic (A). The first rule on the table (HHHH) corresponds to the standard homeostatic rules presented in **Fig. 2**, where all weights obey homeostatic learning. All rules were tested for stability analytically and numerically. A red dot implies that the listed condition is not satisfied, while a green dot means that it does. The condition on the first column indicates whether a stability region for the learning rule is present. The second column indicates whether such region has a large overlap with the region of stability of the neural subsystem. The third column indicates whether the rule is successful, using numerical simulations, at driving the network to a stable Up-state when starting from regimes with self-sustained activity already present (meaning the network is initialized in the linear regime). The fourth column indicates the same as the former, but with the network initialized in the sub-linear regime, where activity is not initially present (e.g., as observed early in developmental conditions).

- (B) Schematic (top) of the population rate model in which the four weights are governed by the HAAA rule in panel (A).
- (C) Example simulation of the HAAA rule over the course of simulated development. The evolution of the firing rate of the excitatory and inhibitory population within a trial in response to a brief external input is shown in every plot.  $E_{set}=5$  and  $I_{set}=14$  represent the target homeostatic setpoints. Weights were initialized to  $W_{EE}=2.1$ ,  $W_{EI}=3$ ,  $W_{IE}=4$ , and  $W_{II}=2$  as in **Fig. 2**. Note that while an evoked Up-state emerges by Trial 200 the firing rates do not converge to their setpoints, and by Trial 500 the Up-state is no longer observed.
- (D) Average rate across trials (upper plot) for the excitatory and inhibitory populations for the data shown in (C). Weight dynamics (bottom plot) produced by the homeostatic rules across trials for the data shown in (C).
- (E) Average final rate for 100 independent HAAA simulations with different weight initializations. Those initializations included cases in which the network starts in the sublinear regime (where the initial  $E$  firing rate was zero or very low). The weights were initialized uniformly between the following ranges:  $W_{EE}[1,3]$ ,  $W_{EI}[0.5,1.5]$ ,  $W_{IE}[4,8]$ ,  $W_{II}[0.2,0.8]$ . Data represents mean  $\pm$  SEM.
- (F) Analytical stability regions of the neural and HAAA learning rule subsystems as a function of the free weights  $W_{EE}$  and  $W_{IE}$ . Here the stability plot is obtained by considering equal learning rates for all four learning rules (as used for panels C-E).
- (G) Similar to F but with but with  $\alpha_E \ll \alpha_I$ . Right of blue line shows the area where the network is in a paradoxical regime (defined by the condition  $W_{EE} * g_E - 1 > 0$ ). Contrary to standard homeostatic rules (**Fig. 2**), the HAAA rule is only stable in the paradoxical region of parameter space (i.e.,  $W_{EE} * g_E - 1 > 0$ ; note white area to the left of the blue line). This may explain why the rule fails at driving the network to an Up-state when starting with developmental-like conditions.

## REFERENCES

- Antoine MW, Langberg T, Schnepel P, Feldman DE (2019) Increased Excitation-Inhibition Ratio Stabilizes Synapse and Circuit Excitability in Four Autism Mouse Models. *Neuron* 101:648-661.e644.
- Bartram J, Kahn MC, Tuohy S, Paulsen O, Wilson T, Mann EO (2017) Cortical Up states induce the selective weakening of subthreshold synaptic inputs. *Nature Communications* 8:665.
- Beltramo R, D'Urso G, Dal Maschio M, Farisello P, Bovetti S, Clovis Y, Lassi G, Tucci V, De Pietri Tonelli D, Fellin T (2013) Layer-specific excitatory circuits differentially control recurrent network dynamics in the neocortex. *Nat Neurosci* 16:227-234.
- Blein S, Hawrot E, Barlow P (2000) The metabotropic GABA receptor: molecular insights and their functional consequences. *Cell Mol Life Sci* 57:635-650.
- Bolz J (1994) Cortical circuitry in a dish. *Curr Opin Neurobio* 4:545-549.
- Brunel N (2000) Dynamics of networks of randomly connected excitatory and inhibitory spiking neurons. *Journal of Physiology-Paris* 94:445-463.
- Buonomano DV, Merzenich MM (1998) Cortical plasticity: from synapses to maps. *Annual Rev Neuroscience* 21:149-186.
- Burrone J, O'Byrne M, Murthy VN (2002) Multiple forms of synaptic plasticity triggered by selective suppression of activity in individual neurons. *Nature* 420:414-418.
- Buzsáki G, Mizuseki K (2014) The log-dynamic brain: how skewed distributions affect network operations. *Nature Reviews Neuroscience* 15:264-278.
- Chiu CQ, Barberis A, Higley MJ (2019) Preserving the balance: diverse forms of long-term GABAergic synaptic plasticity. *Nature Reviews Neuroscience* 20:272-281.
- Chiu CQ, Martenson JS, Yamazaki M, Natsume R, Sakimura K, Tomita S, Tavalin SJ, Higley MJ (2018) Input-Specific NMDAR-Dependent Potentiation of Dendritic GABAergic Inhibition. *Neuron* 97:368-377.e363.
- De Simoni A, Griesinger CB, Edwards FA (2003) Development of rat CA1 neurones in acute versus organotypic slices: role of experience in synaptic morphology and activity. *J Physiol* 550:135-147.
- Douglas RJ, Koch C, Mahowald M, Martin K, Suarez HH (1995) Recurrent excitation in neocortical circuits. *Science* 269:981-985.
- Drew PJ (2019) Vascular and neural basis of the BOLD signal. *Current Opinion in Neurobiology* 58:61-69.
- Echevarria D, Albus K (2000) Activity-dependent development of spontaneous bioelectric activity in organotypic cultures of rat occipital cortex. *Brain Res Dev Brain Res* 123:151-164.
- Fanselow EE, Connors BW (2010) The Roles of Somatostatin-Expressing (GIN) and Fast-Spiking Inhibitory Interneurons in up-down States of Mouse Neocortex. *Journal of Neurophysiology* 104:596-606.
- Field RE, D'amour JA, Tremblay R, Miehl C, Rudy B, Gjorgjieva J, Froemke RC (2020) Heterosynaptic Plasticity Determines the Set Point for Cortical Excitatory-Inhibitory Balance. *Neuron* 106:842-854.e844.
- Froemke RC (2015) Plasticity of Cortical Excitatory-Inhibitory Balance. *Annual Review of Neuroscience* 38:195-219.
- Froemke RC, Merzenich MM, Schreiner CE (2007) A synaptic memory trace for cortical receptive field plasticity. *Nature* 450:425-429.
- Fuster JM, Jervey JP (1981) Inferotemporal neurons distinguish and retain behaviorally relevant features of visual stimuli. *Science* 212:952-955.
- Gainey MA, Aman JW, Feldman DE (2018) Rapid Disinhibition by Adjustment of PV Intrinsic Excitability during Whisker Map Plasticity in Mouse S1. *The Journal of Neuroscience* 38:4749-4761.
- Goel A, Buonomano DV (2016) Temporal interval learning in cortical cultures is encoded in intrinsic network dynamics. *Neuron* 91:320-327.

- Goel A, Lee H-K (2007) Persistence of Experience-Induced Homeostatic Synaptic Plasticity through Adulthood in Superficial Layers of Mouse Visual Cortex. *J Neurosci* 27:6692-6700.
- Goldman-Rakic PS (1995) Cellular basis of working memory. *Neuron* 14:477-485.
- Goold CP, Nicoll RA (2010) Single-Cell Optogenetic Excitation Drives Homeostatic Synaptic Depression. *Neuron* 68:512-528.
- Haider B, Duque A, Hasenstaub AR, McCormick DA (2006) Neocortical Network Activity In Vivo Is Generated through a Dynamic Balance of Excitation and Inhibition. *J Neurosci* 26:4535-4545.
- Hartman KN, Pal SK, Burrone J, Murthy VN (2006) Activity-dependent regulation of inhibitory synaptic transmission in hippocampal neurons. *Nat Neurosci* 9:642-649.
- Hebb DO (1949) *Organization of behavior*. New York: Wiley.
- Hengen Keith B, Torrado Pacheco A, McGregor James N, Van Hooser Stephen D, Turrigiano Gina G (2016) Neuronal Firing Rate Homeostasis Is Inhibited by Sleep and Promoted by Wake. *Cell* 165:180-191.
- Hromádka T, Zador AM, DeWeese MR (2013) Up states are rare in awake auditory cortex. *Journal of Neurophysiology* 109:1989-1995.
- lascone DM, Li Y, Sümbül U, Doron M, Chen H, Andreu V, Goudy F, Blockus H, Abbott LF, Segev I (2020) Whole-neuron synaptic mapping reveals spatially precise excitatory/inhibitory balance limiting dendritic and somatic spiking. *Neuron*.
- Jercog D, Roxin A, Barthó P, Luczak A, Compte A, de la Rocha J (2017) UP-DOWN cortical dynamics reflect state transitions in a bistable network. *eLife* 6:e22425.
- Johnson HA, Buonomano DV (2007) Development and Plasticity of Spontaneous Activity and Up States in Cortical Organotypic Slices. *J Neurosci* 27:5915-5925.
- Joseph A, Turrigiano GG (2017) All for One But Not One for All: Excitatory Synaptic Scaling and Intrinsic Excitability Are Coregulated by CaMKIV, Whereas Inhibitory Synaptic Scaling Is Under Independent Control. *The Journal of Neuroscience* 37:6778-6785.
- Keck T, Scheuss V, Jacobsen RI, Wierenga CJ, Eysel UT, Bonhoeffer T, Hübener M (2011) Loss of sensory input causes rapid structural changes of inhibitory neurons in adult mouse visual cortex. *Neuron* 71:869-882.
- Kilman V, van Rossum MC, Turrigiano GG (2002) Activity deprivation reduces miniature IPSC amplitude by decreasing the number of postsynaptic GABA(A) receptors clustered at neocortical synapses. *J Neurosci* 22:1328-1337.
- Kroener S, Chandler LJ, Phillips PEM, Seamans JK (2009) Dopamine Modulates Persistent Synaptic Activity and Enhances the Signal-to-Noise Ratio in the Prefrontal Cortex. *PLoS ONE* 4:e6507.
- Kuhlman SJ, Olivas ND, Tring E, Ikrar T, Xu X, Trachtenberg JT (2013) A disinhibitory microcircuit initiates critical-period plasticity in the visual cortex. *Nature* 501:543-546.
- Liu JK, Buonomano DV (2009) Embedding Multiple Trajectories in Simulated Recurrent Neural Networks in a Self-Organizing Manner. *J Neurosci* 29:13172-13181.
- Liu Z, Golowasch J, Marder E, Abbott LF (1998) A model neuron with activity-dependent conductances regulated by multiple calcium sensors. *J Neurosci* 18:2309-2320.
- Ma Z, Turrigiano GG, Wessel R, Hengen KB (2019) Cortical Circuit Dynamics Are Homeostatically Tuned to Criticality In Vivo. *Neuron* 104:655-664.e654.
- Mackwood O, Naumann LB, Sprekeler H (2021) Learning excitatory-inhibitory neuronal assemblies in recurrent networks. *eLife* 10:e59715.
- Mahrach A, Chen G, Li N, van Vreeswijk C, Hansel D (2020) Mechanisms underlying the response of mouse cortical networks to optogenetic manipulation. *eLife* 9:e49967.
- Martin SJ, Grimwood PD, Morris RG (2000) Synaptic plasticity and memory: an evaluation of the hypothesis. *Annu Rev Neurosci* 23:649-711.
- McCormick DA (1989) GABA as an inhibitory neurotransmitter in human cerebral cortex. *J Neurophysiol* 62:1018-1027.



- Miller KD, Keller JB, Stryker MP (1989) Ocular dominance column development: analysis and simulation. *Science* 245:605-615.
- Motanis H, Buonomano DV (2015) Delayed in vitro Development of Up States but Normal Network Plasticity in Fragile X Circuits. *Eur J Neurosci* 42:2312-2321.
- Motanis H, Buonomano D (2020) Decreased reproducibility and abnormal experience-dependent plasticity of network dynamics in Fragile X circuits. *Scientific Reports* 10:14535.
- Neske GT, Patrick SL, Connors BW (2015) Contributions of Diverse Excitatory and Inhibitory Neurons to Recurrent Network Activity in Cerebral Cortex. *The Journal of Neuroscience* 35:1089-1105.
- Niswender CM, Conn PJ (2010) Metabotropic Glutamate Receptors: Physiology, Pharmacology, and Disease. *Annual Review of Pharmacology and Toxicology* 50:295-322.
- O'Leary T, Williams AH, Caplan JS, Marder E (2013) Correlations in ion channel expression emerge from homeostatic tuning rules. *Proceedings of the National Academy of Sciences* 110:E2645.
- O'Leary T, Williams Alex H, Franci A, Marder E (2014) Cell Types, Network Homeostasis, and Pathological Compensation from a Biologically Plausible Ion Channel Expression Model. *Neuron* 82:809-821.
- Okun M, Lampl I (2008) Instantaneous correlation of excitation and inhibition during ongoing and sensory-evoked activities. *Nature Neuroscience* 11:535-537.
- Ozeki H, Finn IM, Schaffer ES, Miller KD, Ferster D (2009) Inhibitory Stabilization of the Cortical Network Underlies Visual Surround Suppression. *Neuron* 62:578-592.
- Peng Y-R, Zeng S-Y, Song H-L, Li M-Y, Yamada MK, Yu X (2010) Postsynaptic Spiking Homeostatically Induces Cell-Autonomous Regulation of Inhibitory Inputs via Retrograde Signaling. *The Journal of Neuroscience* 30:16220-16231.
- Plenz D, Kitai ST (1998) Up and down states in striatal medium spiny neurons simultaneously recorded with spontaneous activity in fast-spiking interneurons studied in cortex-striatum-substantia nigra organotypic cultures. *J Neurosci* 18:266-283.
- Renart A, de la Rocha J, Bartho P, Hollender L, Parga N, Reyes A, Harris KD (2010) The Asynchronous State in Cortical Circuits. *Science* 327:587-590.
- Romero-Sosa JL, Motanis H, Buonomano DV (2021) Differential excitability of PV and SST neurons results in distinct functional roles in inhibition stabilization of Up-states. *Journal Of Neuroscience* in press.
- Rossum MCWv, Bi GQ, Turrigiano GG (2000) Stable Hebbian Learning from Spike Timing-Dependent Plasticity. *J Neurosci* 20:8812-8821.
- Rubin Daniel B, Van Hooser Stephen D, Miller Kenneth D (2015) The Stabilized Supralinear Network: A Unifying Circuit Motif Underlying Multi-Input Integration in Sensory Cortex. *Neuron* 85:402-417.
- Rudolph M, Pospischil M, Timofeev I, Destexhe A (2007) Inhibition Determines Membrane Potential Dynamics and Controls Action Potential Generation in Awake and Sleeping Cat Cortex. *J Neurosci* 27:5280-5290.
- Rutishauser U, Slotine J-J, Douglas R (2015) Computation in dynamically bounded asymmetric systems. *PLoS Comput Biol* 11:e1004039.
- Sadeh S, Clopath C (2021) Inhibitory stabilization and cortical computation. *Nature Reviews Neuroscience* 22:21-37.
- Sadovsky AJ, MacLean JN (2014) Mouse Visual Neocortex Supports Multiple Stereotyped Patterns of Microcircuit Activity. *The Journal of Neuroscience* 34:7769-7777.
- Sanchez-Vives MV, McCormick DA (2000) Cellular and network mechanisms of rhythmic recurrent activity in neocortex. *Nat Neurosci* 3:1027-1034.
- Sanzeni A, Akitake B, Goldbach HC, Leedy CE, Brunel N, Histed MH (2020) Inhibition stabilization is a widespread property of cortical networks. *eLife* 9:e54875.
- Seamans JK, Nogueira L, Lavin A (2003) Synaptic Basis of Persistent Activity in Prefrontal Cortex In Vivo and in Organotypic Cultures. *Cerebral Cortex* 13:1242-1250.

- Shu Y, Hasenstaub A, McCormick DA (2003) Turning on and off recurrent balanced cortical activity. *Nature* 423:288-293.
- Sippy T, Yuste R (2013) Decorrelating Action of Inhibition in Neocortical Networks. *The Journal of Neuroscience* 33:9813-9830.
- Slomowitz E, Styr B, Vertkin I, Milshtein-Parush H, Nelken I, Slutsky M, Slutsky I (2015) Interplay between population firing stability and single neuron dynamics in hippocampal networks. *eLife* 4:e04378.
- Song S, Miller KD, Abbott LF (2000) Competitive Hebbian learning through spike-timing-dependent synaptic plasticity. *Nat Neurosci* 3:919-926.
- Steriade M, Contreras D (1998) Spike-Wave Complexes and Fast Components of Cortically Generated Seizures. I. Role of Neocortex and Thalamus. *Journal of Neurophysiology* 80:1439-1455.
- Steriade M, McCormick D, Sejnowski T (1993) Thalamocortical oscillations in the sleeping and aroused brain. *Science* 262:679-685.
- Stoppini L, Buchs P-A, Muller D (1991) A simple method for organotypic cultures of nervous tissue. *Journal of neuroscience methods* 37:173-182.
- Timofeev I, Grenier F, Bazhenov M, Sejnowski TJ, Steriade M (2000) Origin of slow cortical oscillations in deafferented cortical slabs. *Cereb Cortex* 10:1185-1199.
- Trojanowski NF, Bottorff J, Turrigiano GG (2020) Activity labeling in vivo using CaMPARI2 reveals intrinsic and synaptic differences between neurons with high and low firing rate set points. *Neuron*.
- Tsodyks MV, Skaggs WE, Sejnowski TJ, McNaughton BL (1997) Paradoxical Effects of External Modulation of Inhibitory Interneurons. *J Neurosci* 17:4382-4388.
- Turrigiano GG, Nelson SB (2004) Homeostatic plasticity in the developing nervous system. *Nat Neurosci Rev* 5:97-107.
- Turrigiano GG, Leslie KR, Desai NS, Rutherford LC, Nelson SB (1998) Activity-dependent scaling of quantal amplitude in neocortical neurons. *Nature* 391:892-896.
- van Rossum MC, Bi GQ, Turrigiano GG (2000) Stable Hebbian learning from spike timing-dependent plasticity. *J Neurosci* 20:8812-8821.
- van Vreeswijk C, Sompolinsky H (1998) Chaotic balanced state in a model of cortical circuits. *Neural Comput* 10:1321-1371.
- Vogels TP, Sprekeler H, Zenke F, Clopath C, Gerstner W (2011) Inhibitory Plasticity Balances Excitation and Inhibition in Sensory Pathways and Memory Networks. *Science* 334:1569-1573.
- Wang X-J (2001) Synaptic reverberation underlying mnemonic persistent activity. *Trends Neurosci* 24:455-463.
- Wilson HR, Cowan JD (1972) Excitatory and Inhibitory Interactions in Localized Populations of Model Neurons. *Biophysical Journal* 12:1-24.
- Xu H, Jeong H-Y, Tremblay R, Rudy B (2013) Neocortical Somatostatin-Expressing GABAergic Interneurons Disinhibit the Thalamorecipient Layer 4. *Neuron* 77:155-167.
- Xue M, Atallah BV, Scanziani M (2014) Equalizing excitation-inhibition ratios across visual cortical neurons. *Nature* 511:596-600.
- Zucca S, D'Urso G, Pasquale V, Vecchia D, Pica G, Bovetti S, Moretti C, Varani S, Molano-Mazón M, Chiappalone M, Panzeri S, Fellin T (2017) An inhibitory gate for state transition in cortex. *eLife* 6:e26177.